

**Platinum (II) Binuclear Complexes: Molecular Structures,  
Photophysical Properties, and Applications**

Journal:	<i>Journal of Materials Chemistry C</i>
Manuscript ID	TC-REV-03-2019-001585.R1
Article Type:	Review Article
Date Submitted by the Author:	17-Apr-2019
Complete List of Authors:	Chaaban, Maya; Florida State University Zhou, Chenkun; Florida State University, Chemical and Biomedical Engineering Lin, Haoran; Florida State University Chyi, Brandon ; Lawton Chiles High School Ma, Biwu; Florida State University, Chemical and Biomedical Engineering



# Platinum (II) Binuclear Complexes: Molecular Structures, Photophysical Properties, and Applications

Maya Chabaan<sup>a†</sup>, Chenkun Zhou<sup>b†</sup>, Haoran Lin<sup>a</sup>, Brandon Chyi<sup>c</sup>, Biwu Ma<sup>\*abd</sup>

Received 00th January 20xx,  
Accepted 00th January 20xx

DOI: 10.1039/x0xx00000x

www.rsc.org/

Platinum (II) binuclear complexes containing two platinum centers bridged by different types of ligands have received great research attentions for their unique properties and potential applications in a variety of areas. The properties of these binuclear Pt(II) complexes, which could be significantly different from those of their mononuclear counterparts, are highly tunable by modifying their cyclometallating ligands and bridging ligands, as well as the structural configurations. The photophysical properties of these complexes involving a wide range of spectroscopic phenomena make them a very interesting class of materials to be spectroscopically studied. Applications of platinum (II) binuclear complexes have been explored in several areas, ranging from light emitting diodes, to sensors and photocatalysis. In this review, the molecular structures, photophysical properties, and applications of a variety of platinum (II) binuclear complexes are discussed. We intend to shed a light on the recent progress in this field and give a future outlook.

## Introduction

Luminescent transition metal complexes have received tremendous research attentions due to their use in a wide range of applications, such as optical chemosensors,<sup>1-7</sup> photocatalysis,<sup>8-15</sup> bioimaging,<sup>16-21</sup> and organic light emitting diodes (OLEDs).<sup>22-38</sup> The presence of heavy atoms in these complexes promote the intersystem crossing from the singlet to the triplet excited states, enabling them to generate efficient phosphorescence upon excitation.<sup>39, 40</sup> The excited-state dynamics and phosphorescent properties of this class of materials depend on many factors, e.g., the type of metal center, the electronic structure and bulkiness of their ligands,

and their external environments (e.g. temperature, viscosity, etc.).<sup>40, 41</sup> The great structural tunability offers a large number of organometal complexes involving different types of charge transfer transitions<sup>42</sup>, including metal-to-ligand charge transfer (MLCT), ligand-to-ligand charge transfer (LLCT), metal-metal-to-ligand charge transfer (MMLCT), ligand-to-metal charge transfer (LMCT), and intra-ligand charge transfer (ILCT) (Figure 1).<sup>16, 18, 19, 40, 42</sup>

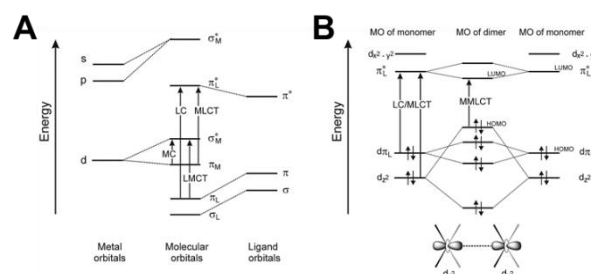


Figure 1 A) Generic molecular orbital diagram for transition metal complexes and relative spectroscopic excitation transitions. B) Simplified molecular orbital diagram of two interacting square-planar platinum (II) complexes, showing the overlap between the  $d_{x^2-y^2}$  orbitals in the ground-state and its influence on the energy of the molecular orbital levels.

<sup>a</sup> Department of Chemistry and Biochemistry, Florida State University, Tallahassee, Florida 32306, United States.

<sup>b</sup> Department of Chemical and Biomedical Engineering, FAMU-FSU College of Engineering, Tallahassee, Florida 32310, United States

<sup>c</sup> Lawton Chiles High School, Tallahassee, Florida 32312, United States.

<sup>d</sup> Materials Science and Engineering Program, Florida State University, Tallahassee, Florida 32306, United States

† M. C. and C. Z. contribute equally. \*Email - bma@fsu.edu



Ms. Maya Chaaban received her bachelor's degree in Chemistry from the Lebanese University and her master's degree in Chemistry from the American University of Beirut. She is currently a PhD student in Prof. Biwu Ma's group at Florida State University. Her research focuses on the development and study of novel luminescent metal complexes.



Mr. Chenkun Zhou is a Chemical Engineering Ph.D. candidate in Professor Biwu Ma's research group at the FAMU-FSU College of Engineering. He received his B.S. degree in Chemistry from Nanjing University (2014). His research focuses on synthetic control of novel luminescent systems, including low-dimensional organic metal halide hybrids and multi-excited-state phosphorescent molecules.

Reproduced with permission from ref. <sup>42</sup>, copyright 2014 Royal Society of Chemistry.

Among these luminescent transition metal complexes,  $d^8$  Pt(II) complexes with square-planar geometry exhibit photophysical properties significantly different from that of  $d^6$  transition metal complexes with pseudo-octahedral geometry.<sup>22,43</sup> The planarity of the Pt(II) complexes makes it possible to have intermolecular interaction between the monomer complexes to form excimers with red-shifted emission.<sup>22, 25, 44, 45</sup> The charge transfer transitions in excimers are usually attributed to MMLCT or LLCT transitions that are strongly dependent on the Pt-Pt distance. In binuclear Pt complexes, the Pt atoms are bridged by ligands (e.g. pyrazole), making intramolecular Pt-Pt interactions possible. According to their bridging-ligand rigidity and structural conformations, the binuclear Pt(II) complexes can be divided into three categories: i) binuclear Pt(II) complexes bridged by rigid ligands and in conformations that do not favor face-to-face interactions (Figure 2A); ii) binuclear Pt(II) complexes bridged by rigid ligands with strong intramolecular Pt-Pt interactions (Figure 2B); iii) binuclear Pt(II) complexes bridged by non-rigid ligands that exhibit the properties of both monomer and excimer depending on the molecular environments (Figure 2C).<sup>43</sup> Besides the rigidity of bridging ligands and structural conformations, the electronic structure and bulkiness of cyclometalating ligand can also have a significant effect on the photophysical properties of binuclear Pt(II) complexes. In addition to the cyclometalated binuclear Pt(II) complexes, all inorganic binuclear Pt(II) complexes, such as Pt(II)  $\mu$ -diphosphito complex  $[\text{Pt}_2(\text{P}_2\text{O}_5\text{H}_2)_4]^{4-}$  (Pt(pop)) and its derivatives, have also been reported and extensively studied.<sup>46</sup> In this review, we will mainly focus on the unique photophysical and photochemical properties of inorganic binuclear Pt(II) complexes, cyclometalated binuclear Pt(II) complexes, and their derivatives as illustrated in Figure 2B, which have short Pt-Pt distances and strong Pt-Pt interactions. Their applications in devices, including OLEDs, sensing, and photocatalysis will be discussed.

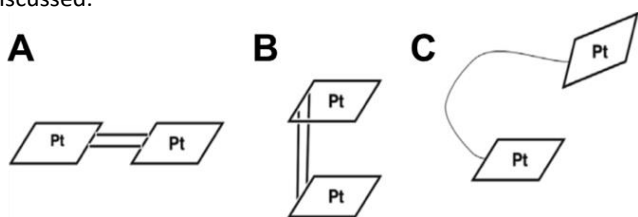


Figure 2 Schematic illustration of the three categories of binuclear complexes. Reproduced with permission from ref.<sup>43</sup>, copyright 2018 Elsevier.

### 1 Pt(pop) and Pt(pop-BF<sub>2</sub>)

Pt(II)  $\mu$ -diphosphito complex  $[\text{Pt}_2(\text{P}_2\text{O}_5\text{H}_2)_4]^{4-}$  known as Pt(pop) is the most extensively studied binuclear Pt(II) complex. The spectroscopic properties of this complex have been well explored since the discovery of its crystal structure in 1980.<sup>47</sup> Each Pt atom is coordinated to four phosphite groups in a square-planar geometry and the two parallel  $\text{P}_4\text{Pt}$  planes are linked with four P-O-P bridges with a Pt-Pt distance of 2.925 Å. The complex exhibits luminescence from both singlet and triplet states due to the electronic transition from the metal-metal antibonding orbital  $5d_{z^2}(\sigma^*)$  to the metal-metal bonding orbital  $6p_z(\sigma)$  that creates  $^1A_{2u}$  and  $^3A_{2u}$  states in an idealized  $D_{4h}$  symmetry. The  $^3A_{2u}$  term splits as a result to spin-orbit coupling into  $E_u$  and  $A_{1u}$  states.<sup>48</sup> Both components are mainly pure triplets ( $^3d\sigma^*p\sigma$ ) with minor contributions either from higher triplets in the case of  $A_{1u}$  or from higher triplets and LMMCT/ $d\pi p\sigma$  singlets in the case of  $E_u$ .<sup>49</sup>

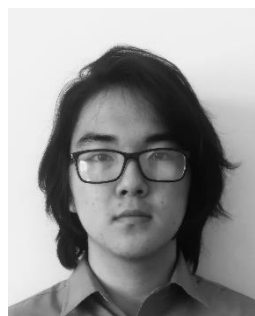
The Pt-Pt orbitals are populated upon excitation, leading to a strong Pt-Pt interaction and a shortening in the Pt-Pt distance of 0.28-0.31 Å.<sup>50</sup> The spectroscopic and photophysical properties of this complex were studied theoretically<sup>51-54</sup> and experimentally using time resolved spectroscopy<sup>55-59</sup>, Raman spectroscopy<sup>60</sup>, transient absorption<sup>61</sup>, and time resolved EXAFS<sup>50, 62</sup>. Pt(pop) exhibits interesting photo reactivity such as hydrogen transfer from organometallic halides<sup>63, 64</sup> and oxidative and reductive quenching by electron transfer processes<sup>65-67</sup>. Recently,  $[\text{Pt}_2(\mu\text{-P}_2\text{O}_5(\text{BF}_2)_2)_4]^{4-}$  (Pt(pop-BF<sub>2</sub>)) a derivative of Pt(pop) was also reported to exhibit dual emission from the singlet and triplet states with a photoluminescent quantum yield (PLQY) approaching unity.<sup>68</sup> (Figure 3A)

#### 1.1 Molecular and Electronic structures of Pt(pop) and Pt(pop-BF<sub>2</sub>)

The conformation of  $d^8$ - $d^8$  bridged complexes are strongly influenced by the geometry of the bridging ligands. In the case of Pt(pop) and Pt(pop-BF<sub>2</sub>), the strain imposed by the bridge is small and the Pt-Pt distance is fixed at 2.93 Å for solid  $\text{Bu}_4\text{N}^+$  and in ethanol solution and at 2.887 Å for solid  $\text{PhAs}_4^+$  salt.<sup>46</sup> Although the Pt-Pt distance is too long to be considered as a bond and the molecular orbital diagram indicates a bond order of zero (Figure 3B), resonance Raman studies suggests that there is certain degree of bonding in the ground state due to the favorable mixing of  $n(d_{z^2})$  and  $(n+1)p_z$  orbitals.<sup>60</sup> Several studies focused on resolving the excited state structure of Pt(pop) and determining the Pt-Pt shortening relying on the metal-metal stretch vibrational frequency in the ground and excited states.<sup>53, 69-72</sup> However, the change in the vibrational frequency resulting from the structural changes of pop ligands



Dr. Haoran Lin received his bachelor's degree in Chemistry from Peking University and his Ph.D. degree in Chemistry from the Hong Kong University of Science and Technology. He is currently a postdoctoral fellow in Prof. Biwu Ma's group at Florida State University. His research interests include light-emitting materials, organic-inorganic hybrids, optoelectronic semiconductors and devices.



Mr. Brandon Chyi is a soon-to-be graduate of Lawton Chiles High School, Tallahassee, Florida. He had an internship in Prof. Biwu Ma's group at Florida State University in 2018. He plans to obtain an undergraduate degree in Chemistry or Physics before pursuing a higher degree in Materials Science and Engineering.

upon photoexcitation were not taken into consideration. Therefore, the calculated Pt-Pt contraction values were significantly shorter than the experimental values determined using time resolved X-ray diffraction. X-ray diffraction technique was also employed in measuring the Pt-Pt shortening that lied between 0.23-0.28 Å depending on the counterions.<sup>73</sup> More recently, time resolved EXAFS spectroscopy was used to study the excited-state structure of Pt(pop).<sup>50</sup> This technique detected for the first time the changes in the ligand coordination bonds. Upon excitation, the Pt-P bond length increases by 0.01 Å, indicating a weaker Pt-P bond. This weakening is attributed to the formation of a shorter Pt-Pt bond that reduces the overlap between Pt  $d_{x^2-y^2}$  and the coordinating ligand orbitals. The measured Pt-Pt contraction value was 0.31 Å, which was relatively close to the previously reported values by time resolved X-ray diffraction XAS<sup>69</sup> and DFT calculations<sup>53</sup>.

DFT calculation showed that Pt(pop) complexes with staggered conformations are more stable than the eclipsed ones in the ground state.<sup>52</sup> These conformers are distinguished by the orientation of the hydrogen bonds surrounding the Pt atom. The Pt(pop-BF<sub>2</sub>) in ground state only has eclipsed conformation with a slightly shorter Pt-Pt distance than that of Pt(pop). The geometries of the lowest singlet and triplet excited states of Pt(pop-BF<sub>2</sub>) are almost identical with ~ 0.18 Å shorter Pt-Pt distance as compared to the ground state. For Pt(pop), the Pt-Pt bond was calculated ~ 0.02 Å shorter in the excited triplet than in the excited singlet.<sup>49</sup>

Pt(pop) and Pt(pop-BF<sub>2</sub>) exhibit similar electronic structural features with comparable character and ordering of the molecular orbitals. The  $5d\sigma^*$  HOMO and  $6p\sigma$  LUMO are largely separated from lower occupied and higher unoccupied orbitals. The key features of the electronic structure are the presence of the ligand localized molecular orbitals below the HOMO and  $5d\pi$  molecular orbitals at lower energy. The occupied molecular orbitals are 0.1-0.25 eV closer to the HOMO in the case of Pt(pop). These states can be divided into two energetically isolated states, i.e.  $d\sigma^*p\sigma$  excited states with largely singlet and triplet characters and LMMCT states with Pt-Pt  $\pi\pi\sigma$  and  $d\pi\sigma$  contributions. The LMMCT  $d\pi\sigma$  and  $\pi\pi\sigma$  singlets interact with the lowest  $d\sigma^*p\sigma$  triplet and split it to three spin-orbit states. In addition, the  $d\sigma^*p\sigma$  singlet and triplet are second-ordered spin-orbit coupled through  $^3d\pi\sigma$ /LMMCT, and additionally through  $^1d\pi\sigma$ /LMMCT in the case of Pt(pop). The greater structural flexibility of Pt(pop) leads to the difference in the intersystem crossing (ISC) rates of the two complexes.<sup>49</sup>

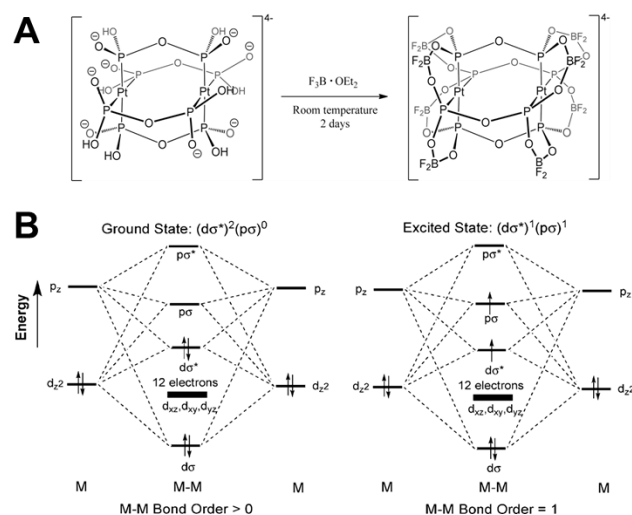


Figure 3 A) Conversion of Pt(pop) to Pt(pop-BF<sub>2</sub>). B) Electronic structures of  $d^8-d^8$  complexes in the ground (left) and lowest triplet states (right) Reproduced with permission from ref. <sup>68</sup>, copyright 2012 American Chemical Society.

**1.2 Photophysical properties.** Pt(pop-BF<sub>2</sub>) and Pt(pop) exhibit similar metal center absorption features being attributed to the electronic transition from  $^1A_{1g}$  to  $^1A_{2u}$  and the spin forbidden triplet transition from  $^1A_{1g}$  to  $^3A_{2u}$ . (Figure 4A) This similarity indicates that BF<sub>2</sub> group have little-to-no effect on the metal center transition. However, the weak absorption peak assigned to the mixed-spin transitions of LMCT are slightly blue shifted for Pt(pop-BF<sub>2</sub>) due to the lower energy levels of the ligand orbitals.<sup>49, 68</sup>

Despite the similarity of the absorption spectra, their emissive spectra are quite different. While both complexes exhibit strong long-lived phosphorescence at 512 nm, the fluorescence of Pt(pop-BF<sub>2</sub>) at 393 nm is 3 times stronger and 100 times longer than that from Pt(pop).<sup>68</sup> The fluorescence of the two complexes are temperature dependent and the lifetime was recorded to be around 8-18 ps and 1.6 ns for Pt(POP) and Pt(pop-BF<sub>2</sub>), respectively, at room temperature.<sup>56, 68</sup> Moreover, the intensity ratio of phosphorescence to fluorescence in Pt(pop-BF<sub>2</sub>) varies at different temperatures while maintaining the same total intensity. This behavior suggests that the conversion from singlet to triplet state become more efficient at higher temperature (Figure 4B).<sup>68</sup>

Moreover, the ISC in Pt(pop) is two times slower than that in Pt(pop-BF<sub>2</sub>) because the direct ISC between states of identical symmetries is allowed only in point groups where at least one of the rotation components belongs to the totally symmetric representation (i.e. The ISC is spin-forbidden in  $D_{4h}$  symmetry group). However, the spin-orbit mixing with higher orbitals could make this process partially allowed. The lower energy ligand orbitals of BF<sub>2</sub> increase the ISC activation energy to 2230  $\text{cm}^{-1}$  from 1190  $\text{cm}^{-1}$  in Pt(pop) and make the spin-coupling between  $^3E_u$  and  $^1A_{2u}$  less favorable, leading to a dramatically longer singlet lifetime of Pt(pop-BF<sub>2</sub>).

The spectroscopy and excited-state decay kinetics of Pt(pop-BF<sub>2</sub>) was studied over a very broad temperature range (1.3–310



Dr. Biwu Ma holds a Ph.D. in Materials Science from the University of Southern California (2006). He is currently an associate professor in the Department of Chemistry and Biochemistry at Florida State University. His current research interests lie in organic-inorganic hybrid materials, molecular photophysics and photochemistry, and organic electronics.

K) to determine the factors that control the ISC process.<sup>74</sup> The decay time of fluorescence is nearly temperature-independent up to about 100 K. At higher temperature, two different thermally activated pathways were promoted as vibronic and/or spin-vibronic coupling pathways are activated. These pathways have larger electronic coupling and Franck-Condon overlap between the optically populated singlet and triplet excited states. (Figure 4C)

The ISC of Pt(pop-BF<sub>2</sub>) was also studied using expressions for multiphoton radiationless transitions where a two-channel model was proposed.<sup>75</sup> The ISC go through a thermally-independent direct  $^1A_{2u} \rightarrow ^3A_{2u}$  channel and a thermally activated indirect  $^1A_{2u} \rightarrow ^3X \rightarrow ^3A_{2u}$  channel. The indirect channel has a strong Franck-Condon overlap at high distorting energy mode due to large energy and small displacement between the singlet and triplet state. However, the crossing from  $^1A_{2u}$  to  $^3A_{2u}$  in the indirect channel go through a moderate distorted state along Pt-Pt ( $^3X$ ). The presence of higher energy modes in Pt(pop) than Pt(pop-BF<sub>2</sub>) makes the ISC slower in Pt(POP) via both channels. (Figure 4D)

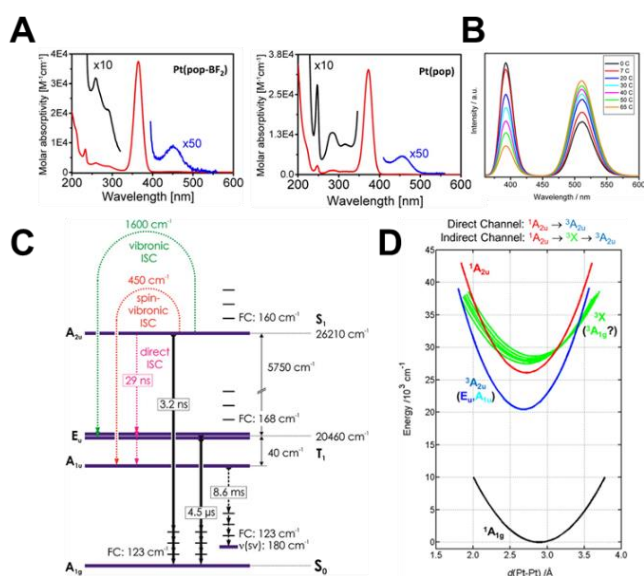


Figure 4 A) Absorption spectra of Pt(pop) and Pt(POP-BF<sub>2</sub>) in acetonitrile. Reproduced with permission from ref.<sup>49</sup>, copyright 2015 American Chemical Society. B) Temperature dependent emission of Pt(POP-BF<sub>2</sub>) in acetonitrile. (excitation at 355 nm) Reproduced with permission from ref.<sup>68</sup>, copyright 2012 American Chemical Society. C) Energy level diagram and relaxation state of the lowest excited state Pt(POP-BF<sub>2</sub>). Reproduced with permission from ref.<sup>74</sup>, copyright 2016 American Chemical Society. D) Approximative energy curves of the ground and excited states of Pt(POP-BF<sub>2</sub>). (The green curves correspond to the estimated positions of the triplet state responsible for the thermally activated ISC process) Reproduced with permission from ref.<sup>75</sup> copyright 2016 American Chemical Society.

**1.3 Electrochemical properties.** Substituting the hydrogens in Pt(pop) by BF<sub>2</sub> groups also affects the electrochemical properties. The electronic-withdrawing nature of BF<sub>2</sub> group stabilizes the dπ energy levels in Pt(pop-BF<sub>2</sub>), making it a

stronger oxidant than Pt(pop). Moreover, the absence of the reducible hydrogen atoms in Pt(pop-BF<sub>2</sub>) makes the reversible reduction of this complex possible. Recently, Darnton et al.<sup>76</sup> reported that Pt(pop-BF<sub>2</sub>) undergoes two 1e<sup>-</sup> reduction to produce the reduced form [Pt<sub>2</sub>(μ-P<sub>2</sub>O<sub>5</sub>(BF<sub>2</sub>)<sub>2</sub>)<sub>4</sub>]<sup>5-</sup> and super-reduced form [Pt<sub>2</sub>(μ-P<sub>2</sub>O<sub>5</sub>(BF<sub>2</sub>)<sub>2</sub>)<sub>4</sub>]<sup>6-</sup>. The first reduction occurs at E<sub>1/2</sub> = -1.68 V and is chemically reversible and electrochemically quasi-reversible. The second reduction occurs at E<sub>p</sub> = -2.46 V vs Fc<sup>+</sup>/Fc and is chemically reversible, but electrochemically irreversible. The d<sup>8</sup> Pt configuration of the complex is not affected by the reductions which make the super-reduced complex a unique 6p<sup>2</sup> σ-bonded binuclear complex. The absorption spectra of the reduced and super-reduced forms of Pt(pop-BF<sub>2</sub>) along with the theoretical calculation and EPR measurements pointed to the successive filling of 6pσ orbitals. The Pt-Pt bond is strengthened upon reduction. However, the rigidity of the ligand prevents the Pt-Pt distance from a significant decrease, which disfavors the overlap between the orbitals; and the presence of six σ electrons in spatial proximity with one another produces a repulsive electronic congestion that weakens the Pt-Pt interaction. The electrochemical properties make Pt(pop-BF<sub>2</sub>) a promising photooxidant for organic reactions.<sup>76</sup>

## 2. Pyrazolate-bridged complexes

Pyrazolate-bridged Pt(II) binuclear complexes, one of the major branches of the family, have received a great deal of interests owing to their unique properties, e.g. controllable charge transfer transition, structural transformation, and dual emission. Unlike Pt(II) monomer complexes exhibiting single emission from ligand centered (LC) and/or MLCT states, many pyrazolate-bridged Pt(II) binuclear complexes possess MMLCT from a filled Pt-Pt antibonding orbital to a vacant ligand-based π\* orbital. The present of MMLCT leads to smaller HOMO-LUMO gaps and red-shifted emission spectra. A series of pyrazolate-bridged cyclometalated Pt(II) complexes reported by our group have shown that the degree of metal-metal interaction and the nature of the excited states can be well controlled by changing the bridging pyrazolate ligands.<sup>77</sup> The Pt-Pt distance was decreased from 3.38 Å to 2.83 Å in the ground state by introducing bulky groups to the 3- and 5-positions of the pyrazolate bridges to force the two cyclometalated Pt moieties closer together, as spectra of [Pt(dfppy)(μ-pz)]<sub>2</sub> (dfppy = 2-(2,4-difluorophenyl)pyridyl, pz = μ-pyrazolate), [Pt(dfppy)(μ-Me<sub>2</sub>pz)]<sub>2</sub> (Me<sub>2</sub>pz = 3,5-dimethylpyrazolate), [Pt(dfppy)(μ-MetBupz)]<sub>2</sub> (MetBupz = 3-methyl-5-tert-butylpyrazolate, and [Pt(dfppy)(μ-tBu<sub>2</sub>pz)]<sub>2</sub> (tBu<sub>2</sub>pz = 3,5-bis(tert-butyl)pyrazolate) (Figure 5B) show bands between 300 and 400 nm that are assigned to MLCT transitions. A lower energy band is observed in [Pt(dfppy)(μ-MetBupz)]<sub>2</sub> and [Pt(dfppy)(μ-tBu<sub>2</sub>pz)]<sub>2</sub> between 400 and 550 nm, which are assigned to MMLCT transitions. The broad absorption bands red-shift as Pt-Pt distance decreases, suggesting the state changing from a mixed <sup>3</sup>LC/MLCT state to low-energy MMLCT. The energy of the d σ\* orbital and the MMLCT excited state show a strong dependence on the metal-metal distance, in which the transition energy decreases with decreasing Pt-Pt

separation. As a result, the emission color of binuclear Pt complexes can be tuned in a rational manner from blue to green and red (Figure 5C).

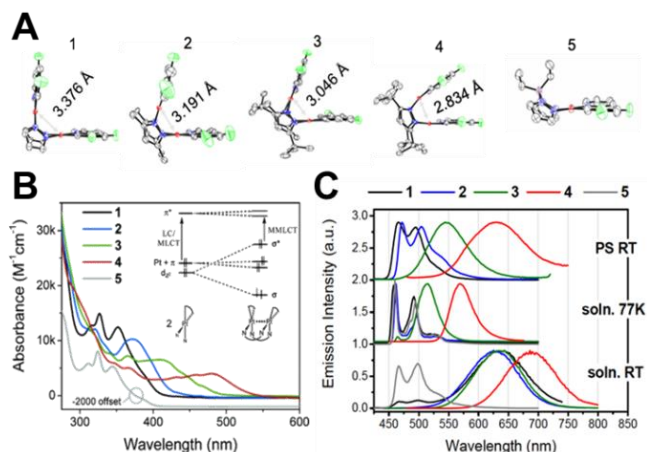


Figure 5 A) A series of binuclear Pt(II) complexes with controlled Pt-Pt distance. B) Absorption spectra for Pt(II) complexes in dichloromethane (DCM) at 298K are shown. Qualitative molecular orbital schemes for  $[\text{Pt}(\text{dfppy})(\mu\text{-pz})_2]$  (**1**),  $[\text{Pt}(\text{dfppy})(\mu\text{-Me}_2\text{pz})_2]$  (**2**),  $[\text{Pt}(\text{dfppy})(\mu\text{-MetBupz})_2]$  (**3**),  $[\text{Pt}(\text{dfppy})(\mu\text{-tBu}_2\text{pz})_2]$  (**4**) and a mononuclear analogue  $\text{dfppyPt}(\text{pz})_2\text{BEt}_2$  ( $\text{BEt}_2 = \text{diethylborane}$ ) (**5**) are shown in the inset. C) Normalized emission spectra of complexes **1-5** in 2-MeTHF solution (bottom and middle) and complexes dispersed in polystyrene at room temperature (top). Reproduced with permission from ref. <sup>77</sup>, copyright 2005 American Chemical Society.

These pyrazolate Pt(II) binuclear complexes were theoretically investigated by DFT calculations to understand why the phosphorescence spectra are significantly depending on the substituents on pyrazolate bridge, as shown in Figure 6.<sup>78,79</sup> The potential energy curves (PECs) were found significantly depend on the bulkiness of substituents on pyrazolate bridge. With small substituents on pyrazolate bridge, one local minimum is present in the  $T_1$  state besides a global minimum. The local minimum geometry is similar to the  $S_0$ -equilibrium one and the triplet excited state here is assigned to  $^3\text{LC}/\text{MLCT}$ . With bulkier tert-butyl substituents on pyrazolate bridge, only the  $T_1$ -global minimum exist. The electronic structure of this  $T_1$ -global minimum is assigned to  $^3\text{MMLCT}$  excited state.

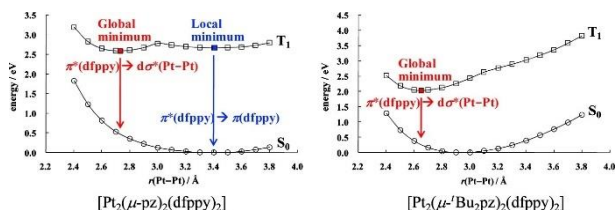


Figure 6. PECs of the  $S_0$  and  $T_1$  states of binuclear complexes versus the Pt-Pt distance in  $[\text{Pt}(\text{dfppy})(\mu\text{-pz})_2]$  and  $[\text{Pt}(\text{dfppy})(\mu\text{-tBu}_2\text{pz})_2]$ . The geometries of the  $S_0$  and  $T_1$  states were optimized with the DFT(B3PW91)/basis-I method at each Pt-Pt distance.

Reproduced with permission from ref. <sup>78</sup>, copyright 2008, American Chemical Society.

Inspired by these early reports on pyrazolate bridged Pt(II) complexes, Castellano and coworkers have investigated the temperature effect on a new  $d^8$ - $d^8$  binuclear Pt(II) chromophore,  $[\text{Pt}(\text{ppy})(\mu\text{-Ph}_2\text{pz})_2]$  (ppy: 2-phenylpyridine;  $\text{Ph}_2\text{pz}$ : 3,5-diphenylpyrazolate).<sup>80</sup> From the temperature dependent emission spectra, the molecule displays mononuclear emission in the temperature range of 77-140 K while appears to exhibit MMLCT emission at above 160K. This suggests that the molecule can undergo a structural reorganization at higher temperature that shortens Pt-Pt distances and enforces Pt-Pt interaction. Further contraction of Pt-Pt distance in the excited state by 0.2-0.3 Å has been observed for pyrazolate-bridged Pt complexes with short Pt-Pt distances by using X-ray spectroscopic techniques, and has also been validated by theoretical calculations.<sup>81-84</sup> Besides bridging pyrazolate groups, cyclometalating ligands have also been demonstrated to play an important role in controlling their photophysical properties.<sup>85</sup> In 2014, our group further studied a pyrazolate bridged Pt(II) binuclear complex,  $[\text{Pt}(\text{dfppy})(\mu\text{-pz})_2]$  (Figure 7A), which has no Pt-Pt interaction in the ground state, but displays interesting dual emission in certain circumstances involving a shortening of the Pt-Pt distance in the excited state.<sup>86</sup> The absorption of  $[\text{Pt}(\text{dfppy})(\mu\text{-pz})_2]$  in DCM at room temperature is shown in Figure 7B. The lowest structured absorption at 462 nm was assigned to the spin-forbidden MLCT transition. This suggests no Pt-Pt interaction and no MMLCT transitions in the ground state. The two dfppy ligands, can be considered the butterfly wings, that remain spread with a long Pt-Pt distance in both the solid state and solution phases. In contrast to the greenish-blue emission observed for  $[\text{Pt}(\text{dfppy})(\mu\text{-pz})_2]$  in a solid-state polystyrene (PS) matrix, dual emission was recorded in DCM solution as shown in Figure 7C. The identical excitation spectra for dual emission suggest that they have the same ground state. The low-energy red emission of  $[\text{Pt}(\text{dfppy})(\mu\text{-pz})_2]$  in solution is almost identical to the emission of  $[\text{Pt}(\text{dfppy})(\mu\text{-tBu}_2\text{pz})_2]$  with short Pt-Pt distance of 2.83 Å in the solid state, suggesting a Pt-Pt distance shortening along with the structural change of  $[\text{Pt}(\text{dfppy})(\mu\text{-pz})_2]$  upon photoexcitation. This induces the formation of a new low-energy excited state. The proposed mechanism of associated with the shortening of the Pt-Pt distance in the excited state is shown in Figure 7D. Upon light absorption,  $[\text{Pt}(\text{dfppy})(\mu\text{-pz})_2]$  is excited to a singlet LC/MLCT excited state ( $S_1$ ), which undergoes ultrafast ISC process to form the first triplet state ( $T_{1a}$ ,  $^3\text{LC}/\text{MLCT}$ ) with a long Pt-Pt distance without Pt-Pt interaction. In the excited state,  $[\text{Pt}(\text{dfppy})(\mu\text{-pz})_2]$  can undergo PSC to form the second low-energy excited state with strong Pt-Pt interaction and red emission ( $T_{1b}$ ,  $^3\text{MMLCT}$ ). Owing to the PSC process and equilibrium between  $T_{1a}$  and  $T_{1b}$ , dual emission in the steady state was achieved for  $[\text{Pt}(\text{dfppy})(\mu\text{-pz})_2]$ .

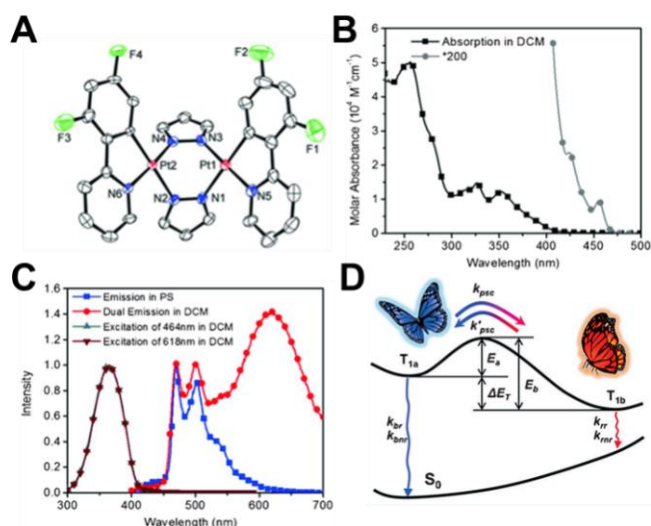


Figure 7 A) The molecular structure of  $[\text{Pt}(\text{dfppy})(\mu\text{-pz})_2]$ . B) Absorption spectrum of  $[\text{Pt}(\text{dfppy})(\mu\text{-pz})_2]$  in DCM at room temperature; the grey line with circles represents a 200-fold magnification of the black line. C) Emission spectra of  $[\text{Pt}(\text{dfppy})(\mu\text{-pz})_2]$  in PS and in DCM at room temperature, and excitation spectra for peak emissions at 464 nm and 618 nm. Reproduced with permission from ref.<sup>86</sup>, copyright 2014, Wiley-VCH. D) Schematic representation of the PSC processes, transitions between various electronic states, and dual emission.  $E_a$  and  $E_b$  are the energy barriers,  $\Delta E_T$  is the energy difference between the  $T_{1a}$  and  $T_{1b}$  states,  $k_{\text{PSC}}$  is the rate of PSC from  $T_{1a}$  to  $T_{1b}$ ,  $k'_{\text{PSC}}$  is the rate of reverse PSC,  $k_{\text{br}}$  and  $k_{\text{rr}}$  are the radiative decay rates of the greenish-blue and red emissions, and  $k_{\text{bnr}}$  (without considering  $k_{\text{PSC}}$ ) and  $k'_{\text{bnr}}$  (without considering  $k'_{\text{PSC}}$ ) are the non-radiative decay rates for  $T_{1a}$  and  $T_{1b}$ . Reproduced with permission from ref.<sup>87</sup>, copyright 2015, Wiley-VCH.

**2.1 Bulkiness Effect.** To realize precise control of the PSC process, a family of butterfly-like phosphorescent binuclear Pt complexes, as shown in Figure 8A, were designed and synthesized by our group to exhibit tunable dual emission of greenish-blue and red light in the steady state.<sup>87</sup> The unique butterfly-like structure of these complexes allows the control of dual emission in two ways, i.e. changing the cyclometallating ligand and the pyrazolate bridge. As shown in Figure 8B, all the seven molecules show greenish-blue emission in PS for the structural reorganization is restricted in solid state. While in DCM solution, dual emission with tunable red/blue ratios were clearly observed. Combined with the theoretical results, the bulkier pyrazolate bridge was found to shift the lowest  $S_0$  state to a shorter Pt-Pt distance at the wing-spreading state and stabilizes  $S_0$  at a short Pt-Pt distance at the wing-folding state. Bulkier cyclometallating ligands have little to no impact on the  $S_0$  state at the wing-spreading state, but destabilize  $S_0$  at the wing-folding state, as illustrated in Figure 8C. The PSC process can be considered as a chemical-reaction-like process occurring on the first triplet excited-state PES, with  $T_{1a}$  as the reactant and  $T_{1b}$  as the product. A nearly linear correlation between the

energy barrier  $E_a$  and the energy difference  $\Delta E_T$  between  $T_{1a}$  and  $T_{1b}$  is observed experimentally and theoretically, conforming to Bell-Evans-Polanyi principle. This relationship suggests that the energy barrier  $E_a$  can be well manipulated by tuning the energy difference  $\Delta E_T$ . (Figure 8D) As a result, a quantitative relationship between the energy barrier and the dual emission color has been demonstrated.

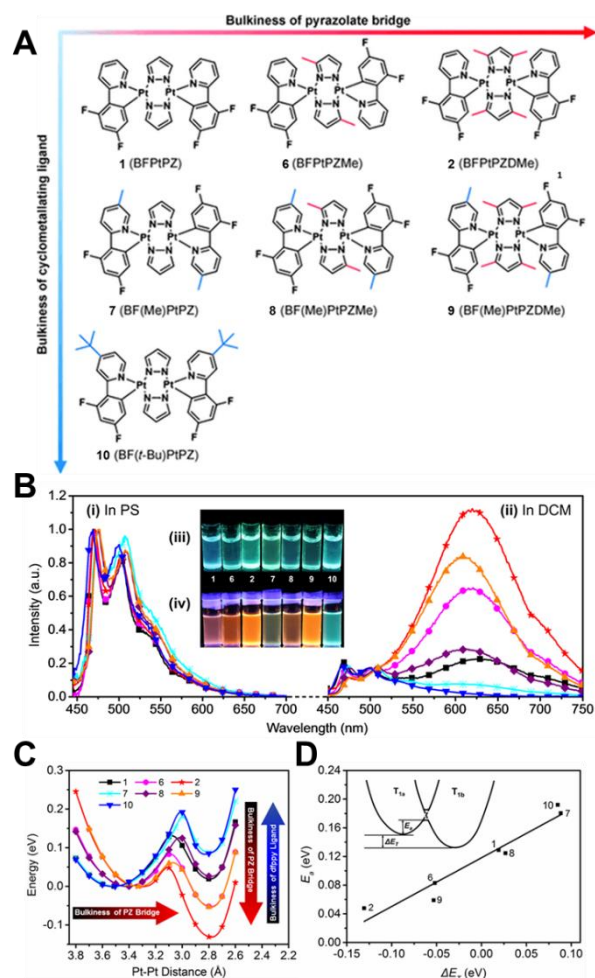


Figure 8 A) Chemical structures of pyrazolate-bridged binuclear platinum complexes with dfppy based ligands as the butterfly wings and pyrazolate ligands as the butterfly body. B) Normalized emission spectra of molecular butterflies (i) in the solid state (in PS) and (ii) in DCM solution at room temperature. iii, iv) Photographs of molecular butterflies (iii) in PS and (iv) in DCM solution under UV light. C) Calculated potential energy surfaces of the first triplet excited state versus the Pt-Pt distance for the molecular butterflies. D) Bell-Evans-Polanyi plots of the energy barrier ( $E_a$ ) versus the energy difference between  $T_{1a}$  and  $T_{1b}$  ( $\Delta E_T$ ). The inset illustrates the Bell-Evans-Polanyi principle. Reproduced with permission from ref.<sup>87</sup>, copyright 2015, Wiley-VCH.

**2.2 Electronic structure effect.** In addition to steric bulkiness effects, a new controlling factor, the electronic structure of the cyclometallating ligand was introduced to manipulate the PESs of this class of molecular butterflies (Figure 9A).<sup>88</sup> As compared to dfppy ligand, two cyclometallating ligands, 2-phenylpyridine

(ppy) and 1-phenylisoquinoline (piq), have different electronic structures. As shown in Figure 9B, ppy has a  $\pi$  molecular orbital on a higher energy level than that of dfppy while the  $\pi^*$  molecular orbital remains on the same energy level. As a result, ppy-based Pt complexes are expected to have a lower  $^3\text{LC}/\text{MLCT}$  transition energy than dfppy-based Pt complexes but the same  $^3\text{MMLCT}$  transition energy. For piq Pt complexes, the  $\pi^*$  orbitals have lower energy which results in smaller  $^3\text{LC}/\text{MLCT}$  and  $^3\text{MMLCT}$  for with shorter Pt-Pt distance. Combining the synthetic control of steric bulkiness of the pyrazolate bridging ligand and the electronic structure of the cyclometallating ligand,  $T_{1a}$  and  $T_{1b}$  can be easily controlled as shown in Figure 9C. As a result, the dual emission peaks can be red-shifted to different emission territories, as shown in Figure 9D.

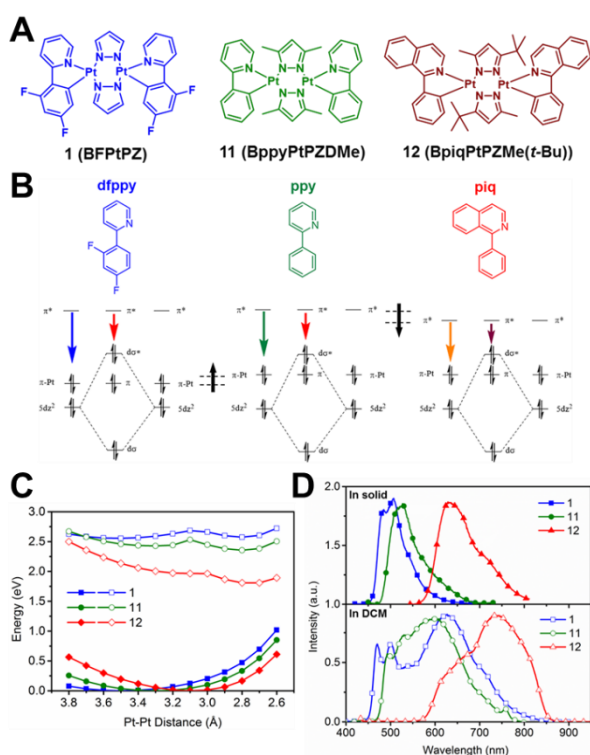


Figure 9 A) Chemical structures of three dual-emissive binuclear Pt(II) complexes with different electronic structures of cyclometallating ligands. B) Simplified molecular orbital diagrams of platinum complexes with different cyclometallating ligands: dfppy, ppy, and piq. The  $^3\text{LC}/\text{MLCT}$  ( $\pi\text{-Pt}\rightarrow\pi^*$ ) and  $^3\text{MMLCT}$  ( $d\sigma^*\rightarrow\pi^*$ ) are dependent on the electronic structure of the cyclometallating ligand. C) Calculated PESs of the first triplet excited state and ground state versus the Pt-Pt distance for the molecular butterflies  $[\text{Pt}(\text{dfppy})(\mu\text{-pz})_2]$  (**1**),  $[\text{Pt}(\text{ppy})(\mu\text{-Me}_2\text{pz})_2]$  (**11**),  $[\text{Pt}(\text{piq})(\mu\text{-MetBupz})_2]$  (**12**). D) Normalized emission spectra of molecular butterflies in the solid state (top, no solvent) and in DCM solution (bottom) at room temperature. Reproduced with permission from ref.<sup>88</sup>, copyright 2016, American Chemical Society.

**2.3 Environment-dependent properties.** The environment-dependent PSC process and photophysical properties of the bridged Pt(II) binuclear complexes enable them to be used as sensors for solid-liquid phase change or for viscosity mapping.

Ethylene carbonate (EC), a solvent with melting point of 35–38°C, was used as the host to demonstrate the sensing capability of  $[\text{Pt}(\text{dfppy})(\mu\text{-pz})_2]$ , as shown in Figure 10A, B.<sup>86</sup> The emission intensity of  $[\text{Pt}(\text{dfppy})(\mu\text{-pz})_2]$  in EC increases between 550–750 nm after the melting point of EC (around 39°C). The emission intensity returns to its initial level after cooling indicating a reversible molecular structural change. The solvent effect on the PSC process was also investigated by picosecond time-correlated single photon counting measurements.<sup>89</sup> In addition to phase change sensor, the molecular butterflies have also been demonstrated as a viscosity sensor. The increasing of viscosity can be considered as an external steric bulkiness effect, which is similar to the introduction of bulky groups into the cyclometallating ligands. The increasing of viscosity can destabilize the  $T_{1b}$  state, resulting in higher energy barrier between  $T_{1a}$  and  $T_{1b}$  states. Therefore, the  $T_{1a}$  state becomes more favored in an equilibrium state and the dual emission ratio can be used to sense the change in the viscosity. These molecular butterflies have higher sensitivity than conventional viscosity-sensing molecular rotors in certain windows with the capability of detecting viscosity change as little as 0.1 cP. In addition, these new molecules with PSC can perform ratiometric self-referenced viscosity sensing. Moreover, since the solution viscosity is temperature dependent, these molecule butterflies can also be used as temperature sensors. As shown in Figure 10C, the emission of  $[\text{Pt}(\text{ppy})(\mu\text{-Me}_2\text{pz})_2]$  in heptadecane was recorded with continuous increase of the solution temperature from 25 to 60 °C. A clear linear correlation between the red/green ratio and temperature was demonstrated (Figure 10D).<sup>87</sup>

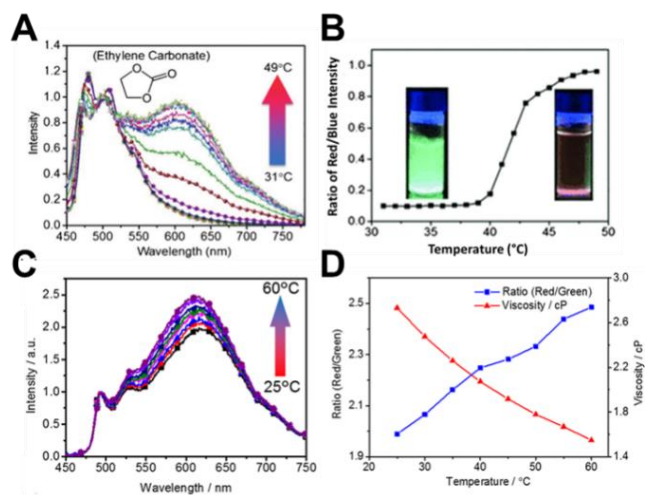


Figure 10 A) Normalized emission spectra of  $[\text{Pt}(\text{dfppy})(\mu\text{-pz})_2]$  in ethylene carbonate at various temperatures from 31°C to 49°C. B) A correlation between the temperature and the ratio of luminescent intensities of peak red emission and greenish-blue emission of  $[\text{Pt}(\text{dfppy})(\mu\text{-pz})_2]$  in ethylene carbonate. Inset: Photographs showing the luminescence in solid ethylene carbonate (left) and in molten ethylene carbonate (right) Reproduced with permission from ref.<sup>86</sup>, copyright 2014, Wiley-VCH. C) Normalized emission spectra of  $[\text{Pt}(\text{ppy})(\mu\text{-Me}_2\text{pz})_2]$  in heptadecane at various temperatures from 25 to 60 °C D) A correlation between the temperature and the ratio of

luminescent intensities of peak red emission and green emission of  $[\text{Pt}(\text{ppy})(\mu\text{-Me}_2\text{pz})_2]$  in heptadecane. Reproduced with permission from ref.<sup>88</sup>, copyright 2016, American Chemical Society.

### 3. Thiolate-bridged complexes

The photophysical properties of thiolate-bridged binuclear Pt(II) complexes were first explored by B. Tzeng et al. in the late 1990s, in an attempt to use these complexes as a model to investigate the interactions between mononuclear Pt(II) thiolate complexes.<sup>90</sup> Following that work, Kato et al. synthesized a new thiolate-bridge binuclear Pt(II) complex that exhibited vapochromic behavior<sup>91</sup>. This complex was isolated in syn- and anti- isomers with head-to-head and head-to-tail configurations respectively, where only the syn-isomer exhibited vapor-induced luminescence switching. This phenomenon was attributed to the presence of a channel in the syn-isomer crystal structure that allowed the penetration of the organic vapor into the structure, which affects the Pt-Pt interaction and the emission. The vapochromism is unique in term of sensitivity since the syn-isomer was found more sensitive to small and less bulky organic molecules. (Figure 11A, B)

Recent studies focused on the thiolate-bridged Pt complexes featuring aromatic C,N cyclometallating ligands. The compounds were generally prepared from chloro-bridged precursors  $\text{Pt}(\text{N}^{\wedge}\text{C})(\mu\text{-Cl})_2$  or from  $\text{Pt}(\text{N}^{\wedge}\text{C})\text{Cl}(\text{HN}^{\wedge}\text{C})$  mononuclear complexes. These complexes have a head-to-tail configuration and exhibit a deep red emission from  $\text{d}\sigma^*\pi^*\text{N}^{\wedge}\text{C}$  MMLCT excited states. This emission is attributed to the rigidity of the metal frameworks with short Pt-Pt distances even in solid state, which enhances the Pt-Pt interaction and shifts the

lowest energy absorption and emission bands to lower energies. V. Sicilia et al. first reported the half-lantern cyclometalated Pt(II)  $[\text{Pt}(\text{bzq})(\mu\text{-C}_7\text{H}_4\text{NS}_2\text{-}\kappa\text{N,S})_2]$  (bzq = benzoquinoline) that shows an efficient and stable <sup>3</sup>MMLCT emission with a quantum yield of 44 % in toluene and 66% in solid state (Figure 11C).<sup>92,93</sup> Later, they evaluated the influence of the thiolate ligand on the photophysical properties of half-lantern cyclometalated Pt(II) complexes by synthesizing  $[\text{Pt}(\text{bzq})(\mu\text{-C}_7\text{H}_4\text{NOS-}\kappa\text{N,S})_2]$  that features 2-mercaptobenzoxazolate (NOS) instead of 2-mercaptobenzothiazolate (NS<sub>2</sub>). The new complex exhibited higher quantum yield (90% in toluene) and a longer Pt-Pt distance that did not affect the energy of the HOMO. On the other hand, the absence of  $\pi\text{-}\pi$  interactions in  $[\text{Pt}(\text{bzq})(\mu\text{-C}_7\text{H}_4\text{NOS-}\kappa\text{N,S})_2]$  destabilized the LUMO and increased the energy of the lower energy electronic absorption, resulting in a more red-shifted emission (Figure 11D). Both complexes can undergo two center two-electron oxidative addition of halogens while conserving the half lantern structure. Z. wang et al. reported a one-pot synthesis of half-lantern cyclometalated Pt(II) complexes featuring 2-phenylpyridine (ppy) as cyclometallating ligand (Figure 11E).<sup>94</sup> The emission from this compound was blue-shifted as compared to the complex containing benzoquinoline (bzq) due to the lower energy of  $\pi^*$  orbital in bzq than that of ppy. The effect of the bridging ligands and cyclometallating ligands was further explored by numerous studies.<sup>95-97</sup> A series of binuclear Pt complexes with a general formula  $[\text{Pt}(\text{N}^{\wedge}\text{C})(\mu\text{-N}^{\wedge}\text{S})_2]$  and their corresponding photophysical properties has been well summarized and reviewed.<sup>43</sup>

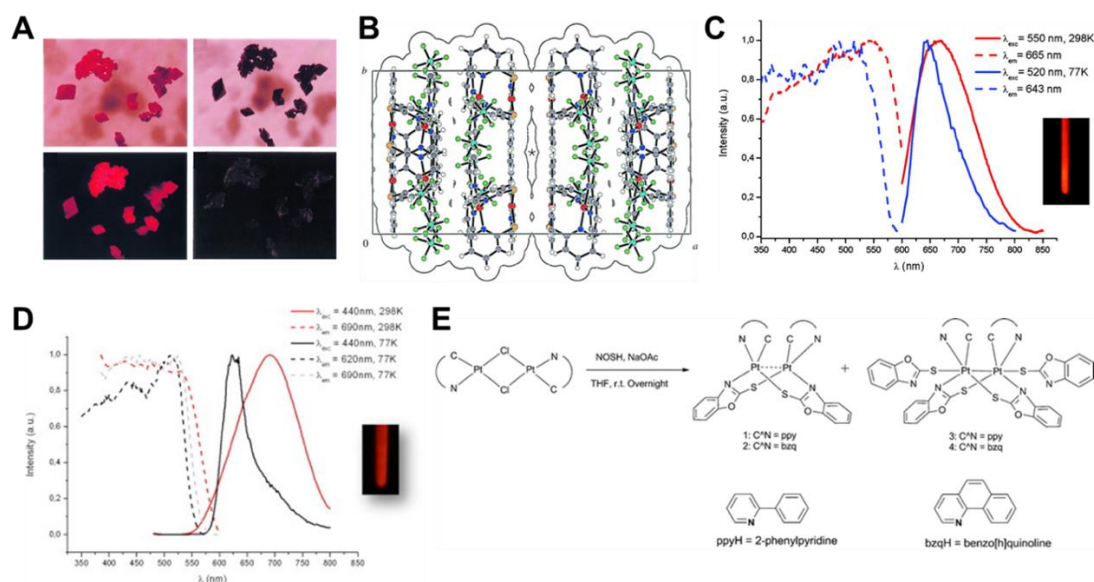


Figure 11 A) Photographic images of crystals of the syn- $[\text{Pt}_2(\text{bpy})_2(\text{pyt})_2][\text{PF}_6]_2$ , illustrating vapochromic effects. B) X-ray packing diagram of syn- $[\text{Pt}_2(\text{bpy})_2(\text{pyt})_2][\text{PF}_6]_2$  (bpy=2,2'-bipyridine, pyt=pyridine-2-thiolate ion) at room temperature with van der Waals outline. Reproduced with permission from ref.<sup>91</sup>, copyright 2002, Wiley-VCH C) Emission spectra of  $[\text{Pt}(\text{bzq})(\mu\text{-C}_7\text{H}_4\text{NS}_2\text{-}\kappa\text{N,S})_2]$  in solid state. Reproduced with permission from ref.<sup>93</sup>, copyright 2012, American Chemical Society. D) emission spectra of  $[\text{Pt}(\text{bzq})(\mu\text{-C}_7\text{H}_4\text{NOS-}\kappa\text{N,S})_2]$  in solid state. Reproduced with permission from ref.<sup>94</sup>, copyright 2012, American Chemical Society. E) Synthesis of binuclear Pt complexes from chloro-bridged precursors using NOSH and NaOAc in THF at room temperature overnight, yielding complexes with ppyH (2-phenylpyridine) or bzqH (benzo[quinoline]thiolate) as cyclometallating ligands.

$C_7H_4NOS-\kappa(N,S)]_2$  in solid state. Reproduced with permission from ref.<sup>92</sup>, copyright 2013, Elsevier. E) One pot synthesis reaction of  $\{Pt(N^A C)(\mu-N^A S)\}_2$  complexes. Reproduced with permission from ref.<sup>94</sup>, copyright 2012, Royal Society of Chemistry.

#### 4. Xanthene, hydroxypridine, and other bridged complexes

Other bridging ligands, such as xanthene, hydroxypridine, quinoline, have been also used to link the Pt units to form binuclear Pt(II) complexes. For instance, S. Develay et al. reported a novel route to obtain highly efficient deep red triplet emitters in solution using xanthene as bridging ligands.<sup>98</sup> Xanthene with high rigidity increase the Pt-Pt interaction to achieve a face-to-face geometry of the Pt units and a unique excimeric emission. Near-IR emission was also reported in a xanthene-bridged complexes structure.<sup>99</sup> The emission of these complexes is highly dependent on the type of solvents and the metal ions (Figure 12A,B). This dependence is associated with the ability of the solvents and metal ions to enhance or compete with the  $\pi$ - $\pi$  interactions. Moreover, a series of red emissive binuclear Pt(II) complexes bridged by large rigid organic molecules xanthene, dibenzofuran, and biphenylene were synthesized and used for  $Pb^{2+}$  sensing.<sup>100</sup> (figure 12C) The  $Pb^{2+}$  ions bind with complexes which affects the  $\pi$ - $\pi$  stacking and leads to a blue-shifted emission. Very recently, two series of binuclear Pt(II) complexes bridged by hydroxypridines and 2-(1H)-quinoline were reported.<sup>101, 102</sup> These complexes exhibited deep red emission from the <sup>3</sup>MMLCT excited state, as shown in figure 12D,E. Among these complexes,  $[Pt(bzq)(\mu-MepyO)]_2$  had the shortest Pt-Pt distance (2.815 Å) ever reported for a <sup>3</sup>MMLCT emitter to date.

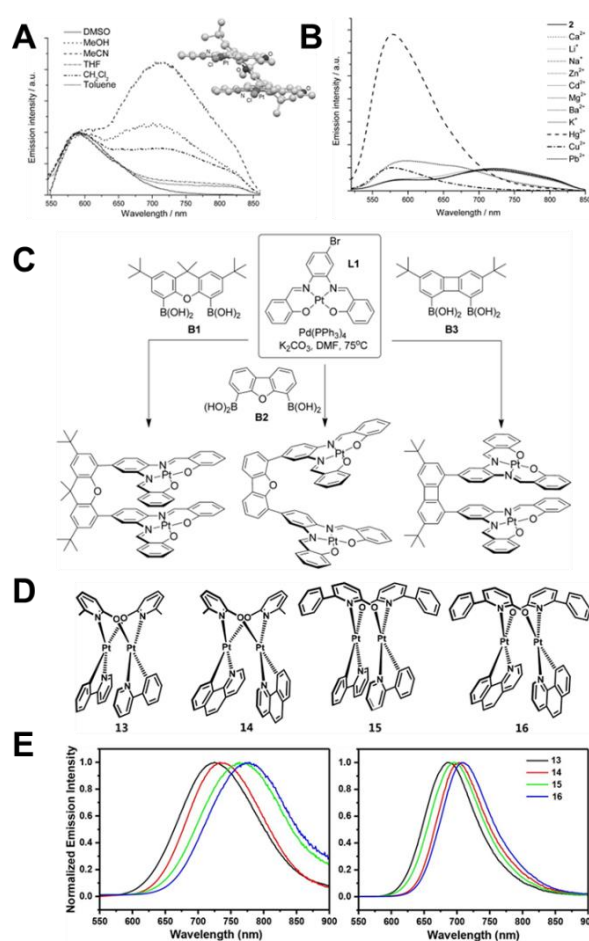


Figure 12 A) Emission spectra for xanthene-bridged complex in different solvents. B) Luminescent spectral change of the same xanthene-bridged complex upon addition of 9.0 equiv. of various metal ions in  $CH_3CN$ . Reproduced with permission from ref.<sup>99</sup>, copyright 2009, Wiley-VCH. C) Synthesis of the binuclear Pt(II) complexes bridged by large rigid organic molecules xanthene, dibenzofuran, and biphenylene. Reproduced with permission from ref.<sup>43</sup>, copyright 2013, Wiley-VCH. D) Structures of the 2-hydroxypyridyl-bridged binuclear Pt(II) complexes anti- $[Pt(ppy)(\mu-MepyO)]_2$  (MepyO=2-hydroxy-6-methylpyridine) (**13**), anti- $[Pt(bzq)(\mu-MepyO)]_2$  (**14**), anti- $[Pt(ppy)(\mu-PhpyO)]_2$  (PhpyO= 2-hydroxy-6-phenylpyridine) (**15**), anti- $[Pt(bzq)(\mu-PhpyO)]_2$  (**16**) E) PL spectra of complexes anti- $[Pt(ppy)(\mu-MepyO)]_2$  (**13**), anti- $[Pt(bzq)(\mu-MepyO)]_2$  (**14**), anti- $[Pt(ppy)(\mu-PhpyO)]_2$  (**15**), anti- $[Pt(bzq)(\mu-PhpyO)]_2$  (**16**) in THF at room temperature (left) and at 77 K in MTHF glasses (right). Reproduced with permission from ref.<sup>77</sup>, copyright 2018, American Chemical Society.

#### 5. Ultrafast spectroscopic studies on binuclear Pt(II) complexes

In order to gain a fundamental understanding of the excited state dynamics and kinetics of the Pt(II) binuclear complexes

with photoinduced structural change, ultrafast spectroscopic techniques were employed to unravel the excited state dynamics such as coherent vibrational dynamics, ISC, and vibrational cooling.<sup>61, 89, 103, 104</sup>

Coherent wavepacket motions were first characterized in Pt(pop) using broadband femtosecond measurements combined with singular value decomposition (SVD) and global fit analysis techniques.<sup>103</sup> This study identified a complete scenario of the excited state dynamics and relaxation (Figure 13A-C). Wave packet dynamics in the  $^1A_{2u}$  state potential with a period of 224 fs, coherence decay and concomitant vibrational cooling in 1-2 ps in the  $^1A_{2u}$  state potential, and ISC on the time scale of 10-30 ps were identified. The latter two processes were found to be solvent dependent. The vibrational relaxation involves energy dissipation to the solvent, likely involving Pt-H interactions along the open axial coordination sites. Despite the large spin-orbit coupling strength of Pt atoms, the ISC rate in Pt(pop) is relatively slow. This can be attributed to the fact that the lowest singlet and triplet state curves are parallel and the direct SO coupling between them is trivial.

More recently, coherent wavepacket motions were also detected in cyclometalated binuclear Pt(II) complexes.<sup>104</sup> Although both binuclear Pt(II) complexes and Pt(pop) exhibit similar structural changes in the excited state, their excited state

dynamics are different because of the presence of MMLCT transition in the binuclear Pt(II) complexes. In this study, L. Chen et al. selected two cyclometalated binuclear Pt(II) complexes (ppy)Pt( $\mu$ -tBu<sub>2</sub>pz)<sub>2</sub> and anti-[(ppy)Pt( $\mu$ -pyt)<sub>2</sub>] (pyt = pyridine-2-thiol) (Figure 13D). The two molecules have two different structures, e.g. the Pt-Pt distance (2.97 Å for (ppy)Pt( $\mu$ -tBu<sub>2</sub>pz)<sub>2</sub> vs 2.85 Å for anti-[(ppy)Pt( $\mu$ -pyt)<sub>2</sub>] and the molecular shapes (H or A frames) where the  $\pi$ - $\pi$  interactions of ppy are more favored in the H frame of anti-[(ppy)Pt( $\mu$ -pyt)<sub>2</sub>] compared with the A frame of (ppy)Pt( $\mu$ -tBu<sub>2</sub>pz)<sub>2</sub>. The increase in  $\pi$ - $\pi$  interactions in the H shape led to a strong vibronic coupling between the MMLCT transitions and the ligand vibrational mode and affected the Pt-Pt stretching frequency. These differences were clearly expressed in their vibrational wavepackets, while (ppy)Pt( $\mu$ -tBu<sub>2</sub>pz)<sub>2</sub> showed one single frequency in the MMLCT state at 120 cm<sup>-1</sup>, anti-[(ppy)Pt( $\mu$ -pyt)<sub>2</sub>] exhibited two down-shifted frequencies in the MMLCT state at 80 and 105 cm<sup>-1</sup>. Additionally, the dephasing time is shorter in anti-[(ppy)Pt( $\mu$ -pyt)<sub>2</sub>], indicating that the triplet PES in anti-[(ppy)Pt( $\mu$ -pyt)<sub>2</sub>] is narrower (Figure 13F). These results indicated that the shape of the molecule is another factor to be considered in controlling the Pt-Pt distance and the interaction between the cyclometalated ligands.

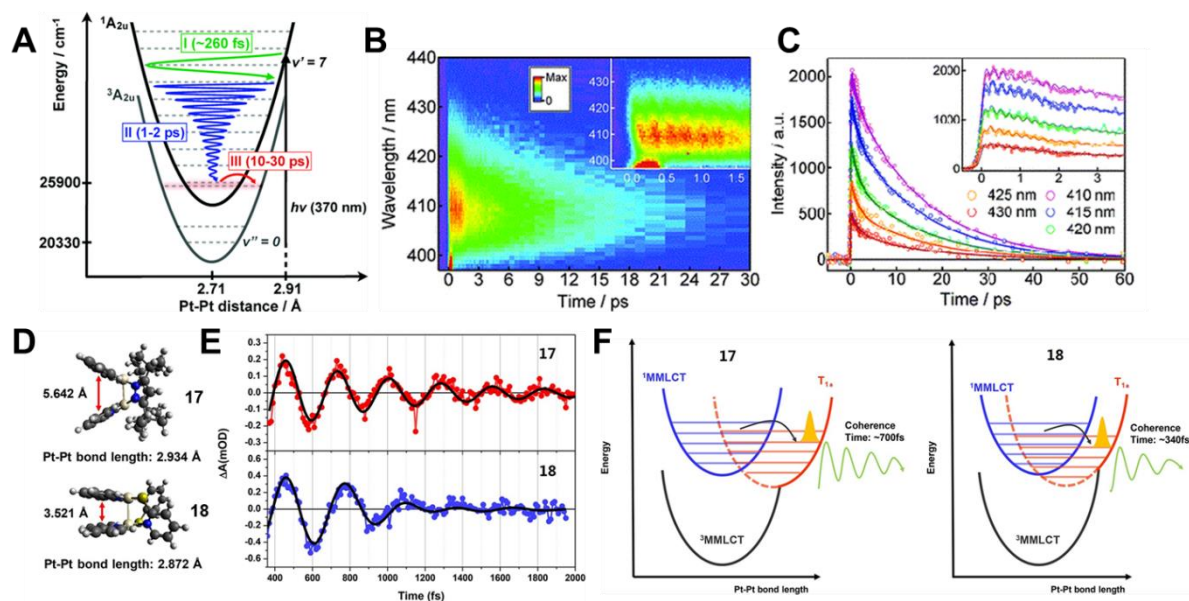


Figure 13 A) Potential energy level diagram summarizing the relative energies and the characteristic time scales of the various relaxation processes for Pt(pop). (I) Impulsive vibrational cooling during the first Pt-Pt oscillation. (II) Solvent-dependent vibrational cooling at a rate of  $\sim 35$  cm<sup>-1</sup>/100 fs and concomitant coherence decay. (III) Intersystem crossing. B) 2D time-wavelength plot of time resolved fluorescence data for Pt(pop) in water excited with a  $\sim 120$  fs laser pulse at 380 nm. The inset shows a zoom into the initial 1.7 ps time window. C) Fluorescence time traces (open circles) at various wavelengths with their fit functions using a global fit model (solid lines). Reproduced with permission from ref. <sup>103</sup>, copyright 2011, American Chemical Society. D) Ball and stick representation of the optimized ground-state structure of (ppy)Pt( $\mu$ -tBu<sub>2</sub>pz)<sub>2</sub> (**17**) and anti-[(ppy)Pt( $\mu$ -pyt)<sub>2</sub>] (**18**). Arrows indicate the center-to-center distance between ppy ligand planes. E) Oscillatory components of (ppy)Pt( $\mu$ -tBu<sub>2</sub>pz)<sub>2</sub> and anti-[(ppy)Pt( $\mu$ -pyt)<sub>2</sub>] observed at 540 nm after subtraction of the solvent contribution, together with the fit to exponentially damped cosine functions. F) Schematic energy relaxation diagram of (ppy)Pt( $\mu$ -tBu<sub>2</sub>pz)<sub>2</sub> and anti-[(ppy)Pt( $\mu$ -pyt)<sub>2</sub>] with PESs in terms of Pt-Pt distance. Reproduced with permission from ref. <sup>104</sup>, copyright 2018, American Chemical Society.

## 6. Applications of binuclear Pt(II) complexes

Phosphorescent Pt(II) complexes are known to have a wide range of application from organic light-emitting diodes (OLEDs), photocatalysis to bioimaging and sensors, which are summarized in a number of reviews.<sup>1, 3, 22, 42, 43, 105-109</sup> These applications benefit from the superior photophysical and photochemical properties of the Pt(II) complexes with great structural diversity. In addition, the properties of these devices based on binuclear Pt(II) complexes could also be finely tuned by controlling the Pt-Pt interaction and the MLCT/MMLCT processes. Despite of their unique and promising properties for different applications, the reports of their applications are lesser than that for their mononuclear counterparts.

Fabrication of OLEDs is one of the most important application of binuclear Pt(II) complexes.<sup>27</sup> The earliest OLED based on binuclear Pt(II) complexes was reported by Saito et al., in which two Pt atoms are bridged by pyridine-2-thiolate ligands.<sup>110</sup> A red emission with maximum luminous efficiency of  $1.8 \text{ cd A}^{-1}$  and an external quantum efficiency (EQE) of 3.4% were obtained. Later, Yu et al. developed another red OLED using binuclear Pt (II) complex bridged with oxadiazole-2-thiol with an EQE of 8.4% and a current efficiency of  $4.2 \text{ cd A}^{-1}$ .<sup>111</sup> The pyridine-2-thiolate based complexes were also used to fabricate NIR OLED devices. For instance, Wu et al. reported NIR LED devices with emission spectrum from 600 to 850 nm, which have maximum EQE of 6.3% and maximum brightness of  $3230 \text{ mW cm}^{-2}$ .<sup>112</sup> Later, Zhu et al. developed a series of oxadiazole-2-thiol bridged complexes to fabricate OLEDs with NIR emission.<sup>113</sup> The highest EQE for these binuclear Pt(II) complex based OLEDs was improved to 8.86%, with a radiant emittance of  $982 \text{ mW cm}^{-2}$ .<sup>114</sup> Color tunability of the OLED devices have been demonstrated by Ma et al. who successfully developed monochromatic blue, green, red and white OLEDs based on color-tunable pyrazolate-bridged Pt(II) binuclear complexes.<sup>115</sup> The color tuning is realized by manipulating the bulkiness of the pyrazolate bridging ligand used to control the intramolecular Pt-Pt separation (Figure 14A-C). Unlike mononuclear Pt complexes with emissions depending on dopant concentration, the electroluminescent spectra of these pyrazolate bridged Pt(II) binuclear complexes only depend on the Pt-Pt distance and independent of the dopant concentration. The blue OLED shows a quantum efficiency of 4.3 % at  $120 \text{ Cd m}^{-2}$ , a brightness of  $3900 \text{ Cd m}^{-2}$  at 12 V, and Commission Internationale de L'Eclairage (CIE) coordinates of (0.11, 0.24). Green and red OLEDs have quantum efficiencies of  $\sim 6.7$  %, with CIE

coordinates of (0.31, 0.63) and (0.59, 0.46), respectively. The white OLEDs based on the combination of two monochromatic complexes have a quantum efficiency of  $\sim 5\%$  and brightness of  $\sim 600 \text{ Cd m}^{-2}$  at 10 V. Another two pyrazolate-bridged Pt(II) binuclear complexes demonstrated by Su et al. exhibited NIR emissions with peaks at around 700 nm.<sup>116</sup> The maximum EQE of 0.15% and maximum radiant intensity of  $19.10 \text{ mW cm}^{-2}$  were obtained in the device based on these molecules. (Figure 14D) The OLEDs based on Pt binuclear complexes using larger bridging ligands were also reported. For example, blue emitting binary triphenylamine-substituted indolo[3,2-b]carbazole was utilized by Yu et al. to connect two planar Pt complex moieties to tune the excimer emission and obtain a white light LED device.<sup>117</sup> A CIE of coordinates of (0.325, 0.345) and a maximum brightness of  $208 \text{ Cd m}^{-2}$  were achieved. Yang et al. also reported OLED devices based on Pt-complexes-anchored polyhedral oligomeric silsesquioxane materials.<sup>118</sup> However, increasing number of Pt complexes bonded to polyhedral oligomeric silsesquioxane macromolecules will result in a worse device performance which was attributed to intramolecular aggregation quenching. (Figure 14E) In addition, binuclear Pt (II) complexes bearing ligands such as acetylacetone and its derivatives were also used in the fabrication of OLEDs.<sup>119-122</sup>

Due to the dependence of Pt-Pt interaction on the environment, Pt(II) binuclear complexes are also perfect candidates for sensing applications.<sup>105</sup> Rachford et al. noticed that three pyrazolate-bridged Pt(II) binuclear complexes exhibit different degrees of temperature-dependent emissions.<sup>80</sup> By decreasing the temperature, the intensity of emission peak at lower energy decreases while the intensity of emission peak at higher energy increases, as shown in Figure 14F. The thermochromic shift was attributed to the intramolecular  $\sigma$  interactions between the two pseudofacial Pt centers. The molecular butterflies developed by our group have also been demonstrated as phase change sensor and temperature sensor.<sup>86</sup> The PSC of these molecules are highly dependent on the temperature. The ratio of the intensity of blue to red peaks is highly dependent on the temperature within a certain temperature window, enabling their use as temperature sensors. Moreover, the family of "molecular butterflies" developed by Zhou et al. have been demonstrated as molecular viscosity sensors since near linear correlation between the ratio of luminescent intensities of the dual emission peaks of these molecules and the viscosity of the solvent was observed.<sup>88</sup>

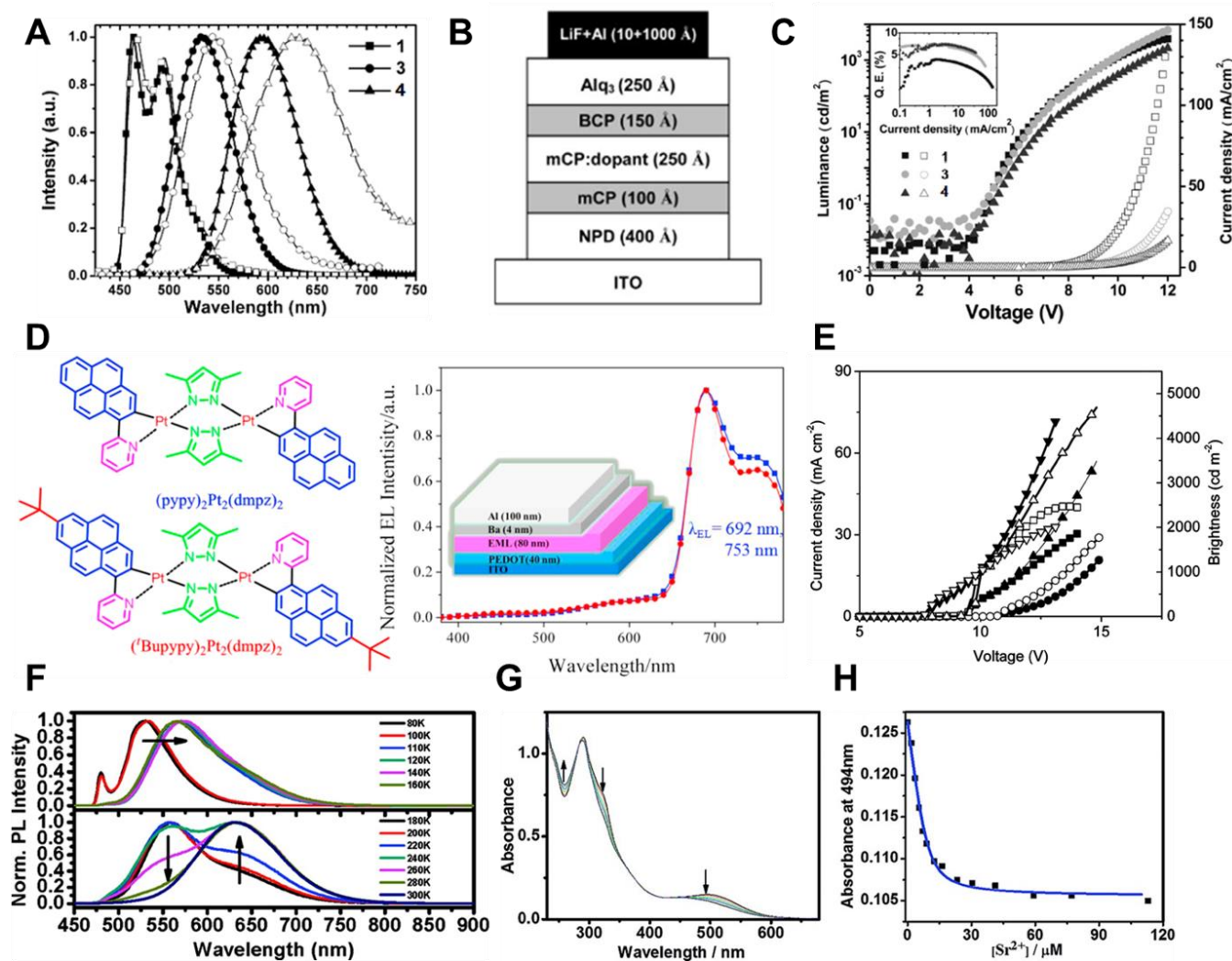


Figure 14 A) Corresponding EL spectra (filled symbols) for OLEDs using compounds [Pt(dfppy)(μ-pz)]<sub>2</sub> (**1**), [Pt(dfppy)(μ-MetBupz)]<sub>2</sub> (**3**), [Pt(dfppy)(μ-tBu<sub>2</sub>pz)]<sub>2</sub> (**4**) and their photoluminescence spectra (empty symbols) in polystyrene B) Device architecture for OLEDs using compounds [Pt(dfppy)(μ-pz)]<sub>2</sub> (**1**), [Pt(dfppy)(μ-MetBupz)]<sub>2</sub> (**3**), [Pt(dfppy)(μ-tBu<sub>2</sub>pz)]<sub>2</sub> (**4**) C) Applied voltage-luminance (filled symbols) and applied voltage-current density (open symbols) characteristics for OLED device using compound [Pt(dfppy)(μ-pz)]<sub>2</sub> (**1**), [Pt(dfppy)(μ-MetBupz)]<sub>2</sub> (**3**), [Pt(dfppy)(μ-tBu<sub>2</sub>pz)]<sub>2</sub> (**4**) Reproduced with permission from ref. <sup>115</sup>, copyright 2006, Wiley-VCH. D) The molecular structure of NIR pyrazolate-bridged Pt(II) binuclear complexes and their corresponding emission. Reproduced with permission from ref. <sup>115</sup>, copyright 2006, Wiley-VCH. E) Current density (solid symbols) and luminance (open symbols) versus bias voltage characteristics of device based on Pt-complexes-anchored polyhedral oligomeric silsesquioxane materials. Reproduced with permission from ref. <sup>118</sup>, copyright 2010, American Chemical Society. F) Photoluminescence temperature dependence of [Pt(ppy)(μ-Ph<sub>2</sub>pz)]<sub>2</sub> in MTHF (10<sup>-5</sup> M; λ<sub>ex</sub>=410 nm). Reproduced with permission from ref. <sup>80</sup>, copyright 2009, American Chemical Society. G) Absorption spectra of binuclear compound (15 μm) in acetonitrile upon the addition of Sr(ClO<sub>4</sub>)<sub>2</sub> (1 equiv.). H) Plot of absorbance at 494 nm as a function of Sr<sup>2+</sup> concentration (0 to 8 equiv.). Reproduced with permission from ref. <sup>123</sup>, copyright 2017, Wiley-VCH.

Other than temperature, viscosity, and solid-liquid phase change sensing, Chan et al. found that Pt(II) binuclear complexes could also be used as luminescent ion sensors.<sup>100</sup> They developed several compounds in which two square-planar Pt(II) complex moieties are connected by large rigid organic bridges. Upon addition of Pb<sup>2+</sup> ions, the oxygen on the Pt binuclear complexes could chelate with Pb<sup>2+</sup> which in turn increased the Pt-Pt distance and result in the blue shift of the emission spectra. It is worth noting that only Pb<sup>2+</sup> ions would give rise to the enhanced luminescence while other metal ions give no or minimum response. By introducing aza[15]crown-5 substituent into Pt binuclear complexes, Chen et al. also developed a supermolecule whose luminescence was selectively sensitive to Sr<sup>2+</sup>.<sup>123</sup> When the Sr<sup>2+</sup> is sandwiched between the crown moieties, the lowest excited state of the supermolecule will change from the non-emissive ligand-to-ligand charge transfer (LLCT) state to the emissive MMLCT triplet state since the LLCT transition from the azacrown-containing acetylide ligand to the (C<sup>∧</sup>N<sup>∧</sup>N) acceptor is shifted to higher energy, and the MMLCT transition becomes the lowest energy absorption. (Figure 14G, H)

Other applications for these Pt binuclear complexes, like photocatalysis for oxygen addition, water-splitting, and other reactions, remain largely underexplored. Several multinuclear Pt complexes were used in such applications. However, the Pt atoms are more like individual catalyzing centers in these cases without any Pt-Pt interactions.<sup>124-126</sup> Exploring the use of Pt binuclear complexes with photoinduced structural change should be of great interest for photodetectors, molecular switches and other applications.

## Remarks and Outlook

Pt(II) binuclear complexes exhibit unique photophysical properties dependent on various factors, such as the type of bridging ligands or cyclometalating ligands, and the molecular shape. Pt(pop) has been investigated as a prototype among these binuclear Pt(II) complexes. Their photophysical properties have been extensively studied since the 1990s. Recently, the advancement in ultrafast time-resolved absorption and emission spectroscopies, as well as X-ray spectroscopy were employed in studying the excited state dynamics and kinetics in Pt(pop) and its derivative. Cyclometalated Pt(II) binuclear complexes adopt electronic structures that are different from Pt(pop). Their photophysical properties are also distinct from their mononuclear counterparts. Their superior photophysical properties and great structural diversity allows these binuclear Pt(II) complexes to be used in a variety of applications, including OLEDs, photosensing, and photocatalysis.

While the properties of Pt binuclear complexes have been extensively studied, there is still a number of issues and challenges to be addressed.

a) To better understand the excited state dynamics and structural change kinetics of these complexes, detailed and fundamental studies of the excited state processes using ultrafast X-ray, transient absorption, and DFT calculations are of great necessity and interest. More comprehensive

study on synthetic approach and design rule will benefit the design and development of novel binuclear Pt(II) complexes with favored properties.

- b) While the mononuclear Pt(II) complexes have been extensively explored in application like OLEDs, bioimaging, photosensors, the binuclear Pt(II) complex based devices are still limited with only a few reports. Pt(II) binuclear complexes offer new and useful photophysical properties that are different from their mononuclear counterparts. e.g. PSC and controlled MMLCT. These properties enable the Pt(II) binuclear complexes to be excellent candidates for a variety of applications, including highly sensitive photosensors, OLEDs with high efficiencies specially in the NIR region.
- c) Investigations on the stability and degradation mechanisms of these complexes in devices are still very limited. Understanding of these mechanisms can help us develop novel materials with improved stability and longer device lifetime.

## Conflicts of interest

There are no conflicts to declare.

## Acknowledgements

This work was supported by National Science Foundation (NSF) [grant number 1664661] and Florida State University Office of Research.

## References

1. K. M.-C. Wong and V. W.-W. Yam, *Coord. Chem. Rev.*, 2007, **251**, 2477-2488.
2. Q. Zhao, F. Li and C. Huang, *Chem. Soc. Rev.*, 2010, **39**, 3007-3030.
3. V. Guerschais and J.-L. Fillaut, *Coord. Chem. Rev.*, 2011, **255**, 2448-2457.
4. M. H. Keefe, K. D. Benkstein and J. T. Hupp, *Coord. Chem. Rev.*, 2000, **205**, 201-228.
5. J. N. Demas and B. A. DeGraff, *Anal. Chem.*, 1991, **63**, 829A-837A.
6. E. R. Carraway, J. N. Demas, B. A. DeGraff and J. R. Bacon, *Anal. Chem.*, 1991, **63**, 337-342.
7. B. Higgins, B. A. DeGraff and J. N. Demas, *Inorg. Chem.*, 2005, **44**, 6662-6669.
8. J. E. McGarrah, Y.-J. Kim, M. Hissler and R. Eisenberg, *Inorg. Chem.*, 2001, **40**, 4510-4511.
9. P. Du, J. Schneider, P. Jarosz and R. Eisenberg, *J. Am. Chem. Soc.*, 2006, **128**, 7726-7727.
10. D. Zhang, L.-Z. Wu, L. Zhou, X. Han, Q.-Z. Yang, L.-P. Zhang and C.-H. Tung, *J. Am. Chem. Soc.*, 2004, **126**, 3440-3441.
11. J.-J. Zhong, Q.-Y. Meng, G.-X. Wang, Q. Liu, B. Chen, K. Feng, C.-H. Tung and L.-Z. Wu, *Chem. Eur. J.*, 2013, **19**, 6443-6450.
12. Y. Zhang, J. L. Petersen and C. Milsmann, *J. Am. Chem. Soc.*, 2016, **138**, 13115-13118.

13. H. Yin, P. J. Carroll, J. M. Anna and E. J. Schelter, *J. Am. Chem. Soc.*, 2015, **137**, 9234-9237.
14. L. A. Büldt and O. S. Wenger, *Chem. Sci.*, 2017, **8**, 7359-7367.
15. C. Yang, F. Mehmood, T. L. Lam, S. L.-F. Chan, Y. Wu, C.-S. Yeung, X. Guan, K. Li, C. Y.-S. Chung, C.-Y. Zhou, T. Zou and C.-M. Che, *Chem. Sci.*, 2016, **7**, 3123-3136.
16. Q. Zhao, C. Huang and F. Li, *Chem. Soc. Rev.*, 2011, **40**, 2508-2524.
17. E. Baggaley, J. A. Weinstein and J. A. G. Williams, *Coord. Chem. Rev.*, 2012, **256**, 1762-1785.
18. D.-L. Ma, H.-Z. He, K.-H. Leung, D. S.-H. Chan and C.-H. Leung, *Angew. Chem. Int. Ed.*, 2013, **52**, 7666-7682.
19. M. P. Coogan and V. Fernández-Moreira, *Chem. Commun.*, 2014, **50**, 384-399.
20. K. K.-W. Lo, M.-W. Louie and K. Y. Zhang, *Coord. Chem. Rev.*, 2010, **254**, 2603-2622.
21. F. L. Thorp-Greenwood, *Organometallics*, 2012, **31**, 5686-5692.
22. J. Kalinowski, V. Fattori, M. Cocchi and J. A. G. Williams, *Coord. Chem. Rev.*, 2011, **255**, 2401-2425.
23. C.-M. Che, C.-C. Kwok, S.-W. Lai, A. F. Rausch, W. J. Finkenzeller, N. Zhu and H. Yersin, *Chem. Eur. J.*, 2010, **16**, 233-247.
24. W.-Y. Wong and C.-L. Ho, *Coord. Chem. Rev.*, 2009, **253**, 1709-1758.
25. S. Huo, J. Carroll and D. A. K. Vezzu, *Asian J. Org. Chem.*, 2015, **4**, 1210-1245.
26. M. A. Baldo, D. O'Brien, Y. You, A. Shoustikov, S. Sibley, M. Thompson and S. Forrest, *Nature*, 1998, **395**, 151-154.
27. Q.-C. Zhang, H. Xiao, X. Zhang, L.-J. Xu and Z.-N. Chen, *Coord. Chem. Rev.*, 2018, **378**, 121-133.
28. J. Lee, H.-F. Chen, T. Batagoda, C. Coburn, P. I. Djurovich, M. E. Thompson and S. R. Forrest, *Nat. Mater.*, 2016, **15**, 92.
29. M. Baldo, M. Thompson and S. Forrest, *Nature*, 2000, **403**, 750-753.
30. M. A. Baldo, D. F. O'Brien, Y. You, A. Shoustikov, S. Sibley, M. E. Thompson and S. R. Forrest, *Nature*, 1998, **395**, 151-154.
31. D. Di, A. S. Romanov, L. Yang, J. M. Richter, J. P. H. Rivett, S. Jones, T. H. Thomas, M. Abdi Jalebi, R. H. Friend, M. Linnolahti, M. Bochmann and D. Credgington, *Science*, 2017, **356**, 159-163.
32. S. Shi, M. C. Jung, C. Coburn, A. Tadler, D. Sylvinson MR, P. I. Djurovich, S. R. Forrest and M. E. Thompson, *J. Am. Chem. Soc.*, 2019, **141**, 3576-3588.
33. R. Hamze, J. L. Peltier, D. Sylvinson, M. Jung, J. Cardenas, R. Haiges, M. Soleilhavoup, R. Jazzar, P. I. Djurovich, G. Bertrand and M. E. Thompson, *Science*, 2019, **363**, 601-606.
34. Y. Zhang, Y. Wang, J. Song, J. Qu, B. Li, W. Zhu and W.-Y. Wong, *Adv. Opt. Mater.*, 2018, **6**, 1800466.
35. G. Zhou, W.-Y. Wong and X. Yang, *Chem. Asian J.*, 2011, **6**, 1706-1727.
36. X. Yang, G. Zhou and W.-Y. Wong, *Chem. Soc. Rev.*, 2015, **44**, 8484-8575.
37. X. Xu, X. Yang, J. Zhao, G. Zhou and W.-Y. Wong, *Asian J. Org. Chem.*, 2015, **4**, 394-429.
38. X. Yang, X. Xu, J.-s. Dang, G. Zhou, C.-L. Ho and W.-Y. Wong, *Inorg. Chem.*, 2016, **55**, 1720-1727.
39. A. Juris, V. Balzani, F. Barigelletti, S. Campagna, P. Belser and A. von Zelewsky, *Coord. Chem. Rev.*, 1988, **84**, 85-277.
40. A. J. Lees, *Chem. Rev.*, 1987, **87**, 711-743.
41. K. Kikuchi, M. Hoshi, T. Niwa, Y. Takahashi and T. Miyashi, *J. Phys. Chem.*, 1991, **95**, 38-42.
42. M. Mauro, A. Aliprandi, D. Septiadi, N. S. Kehr and L. De Cola, *Chem. Soc. Rev.*, 2014, **43**, 4144-4166.
43. E. V. Puttock, M. T. Walden and J. A. G. Williams, *Coord. Chem. Rev.*, 2018, **367**, 127-162.
44. V. W.-W. Yam, V. K.-M. Au and S. Y.-L. Leung, *Chem. Rev.*, 2015, **115**, 7589-7728.
45. K. Li, G. S. Ming Tong, Q. Wan, G. Cheng, W.-Y. Tong, W.-H. Ang, W.-L. Kwong and C.-M. Che, *Chem. Sci.*, 2016, **7**, 1653-1673.
46. H. B. Gray, S. Zálíš and A. Vlček, *Coord. Chem. Rev.*, 2017, **345**, 297-317.
47. M. A. F. D. R. Pinto, P. J. Sadler, S. Neidle, M. R. Sanderson, A. Subbiah and R. Kuroda, *J. Chem. Soc., Chem. Commun.*, 1980, **0**, 13-15.
48. W. A. Fordyce, J. G. Brummer and G. A. Crosby, *J. Am. Chem. Soc.*, 1981, **103**, 7061-7064.
49. S. Zalis, Y. C. Lam, H. B. Gray and A. Vlcek, *Inorg. Chem.*, 2015, **54**, 3491-3500.
50. R. M. van der Veen, C. J. Milne, A. El Nahhas, F. A. Lima, V. T. Pham, J. Best, J. A. Weinstein, C. N. Borca, R. Abela, C. Bressler and M. Chergui, *Angew. Chem. Int. Ed.*, 2009, **48**, 2711-2714.
51. G. Levi, M. Pápai, N. E. Henriksen, A. O. Dohn and K. B. Møller, *J. Phys. Chem. C*, 2018, **122**, 7100-7119.
52. G. I. Gellene and D. M. Roundhill, *J. Phys. Chem. A*, 2002, **106**, 7617-7620.
53. I. V. Novozhilova, A. V. Volkov and P. Coppens, *J. Am. Chem. Soc.*, 2003, **125**, 1079-1087.
54. Q.-J. Pan, H.-G. Fu, H.-T. Yu and H.-X. Zhang, *Inorg. Chem.*, 2006, **45**, 8729-8735.
55. Y. Shimizu, Y. Tanaka and T. Azumi, *J. Phys. Chem.*, 1985, **89**, 1372-1374.
56. A. E. Stiegman, S. F. Rice, H. B. Gray and V. M. Miskowski, *Inorg. Chem.*, 1987, **26**, 1112-1116.
57. S. F. Rice and H. B. Gray, *J. Am. Chem. Soc.*, 1983, **105**, 4571-4575.
58. T. Ikeyama, S. Yamamoto and T. Azumi, *J. Phys. Chem.*, 1988, **92**, 6899-6901.
59. S. J. Milder and B. S. Brunschwig, *J. Phys. Chem.*, 1992, **96**, 2189-2196.
60. C. M. Che, L. G. Butler, H. B. Gray, R. M. Crooks and W. H. Woodruff, *J. Am. Chem. Soc.*, 1983, **105**, 5492-5494.
61. R. Monni, G. Auböck, D. Kinschel, K. M. Aziz-Lange, H. B. Gray, A. Vlček and M. Chergui, *Chem. Phys. Lett.*, 2017, **683**, 112-120.
62. D. J. Thiel, P. Liviš, E. A. Stern and A. Lewis, *Nature*, 1993, **362**, 40.
63. R. M. Bullock and E. G. Samsel, *J. Am. Chem. Soc.*, 1990, **112**, 6886-6898.
64. A. Vlcek and H. B. Gray, *Inorg. Chem.*, 1987, **26**, 1997-2001.
65. J. R. Peterson and K. Kalyanasundaram, *J. Phys. Chem.*, 1985, **89**, 2486-2492.
66. W. B. Heuer, M. D. Totten, G. S. Rodman, E. J. Hebert, H. J. Tracy and J. K. Nagle, *J. Am. Chem. Soc.*, 1984, **106**, 1163-1164.
67. A. D. Kirk and L.-Z. Cai, *Inorg. Chem.*, 1998, **37**, 1051-1059.

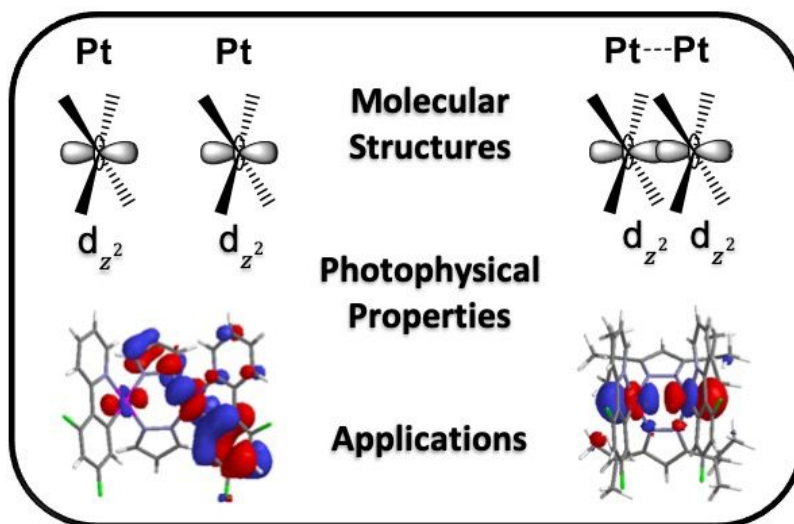
68. A. C. Durrell, G. E. Keller, Y. C. Lam, J. Sykora, A. Vlcek, Jr. and H. B. Gray, *J. Am. Chem. Soc.*, 2012, **134**, 14201-14207.
69. C. D. Kim, S. Pillet, G. Wu, W. K. Fullagar and P. Coppens, *Acta Cryst. A*, 2002, **58**, 133-137.
70. R. M. van der Veen, C. J. Milne, A. El Nahhas, F. A. Lima, V.-T. Pham, J. Best, J. A. Weinstein, C. N. Borca, R. Abela, C. Bressler and M. Chergui, *Angew. Chem.*, 2009, **121**, 2749-2752.
71. M. Christensen, K. Haldrup, K. Bechgaard, R. Feidenhans'l, Q. Kong, M. Cammarata, M. L. Russo, M. Wulff, N. Harrit and M. M. Nielsen, *J. Am. Chem. Soc.*, 2009, **131**, 502-508.
72. D. J. Thiel, P. Livins, E. A. Stern and A. Lewis, *Nature*, 1993, **363**, 565-565.
73. N. Yasuda, H. Uekusa and Y. Ohashi, *Bull. Chem. Soc. Jpn.*, 2004, **77**, 933-944.
74. T. Hofbeck, Y. C. Lam, M. Kalbac, S. Zalis, A. Vlcek, Jr. and H. Yersin, *Inorg. Chem.*, 2016, **55**, 2441-2449.
75. Y. C. Lam, H. B. Gray and J. R. Winkler, *J. Phys. Chem. A*, 2016, **120**, 7671-7676.
76. T. V. Darnton, B. M. Hunter, M. G. Hill, S. Zalis, A. Vlcek, Jr. and H. B. Gray, *J. Am. Chem. Soc.*, 2016, **138**, 5699-5705.
77. B. Ma, J. Li, P. I. Djurovich, M. Yousufuddin, R. Bau and M. E. Thompson, *J. Am. Chem. Soc.*, 2005, **127**, 28-29.
78. K. Saito, Y. Nakao and S. Sakaki, *Inorg. Chem.*, 2008, **47**, 4329-4337.
79. K. Saito, Y. Nakao, K. Umakoshi and S. Sakaki, *Inorg. Chem.*, 2010, **49**, 8977-8985.
80. A. A. Rachford and F. N. Castellano, *Inorg. Chem.*, 2009, **48**, 10865-10867.
81. J. V. Lockard, A. A. Rachford, G. Smolentsev, A. B. Stickrath, X. Wang, X. Zhang, K. Atenkoffer, G. Jennings, A. Soldatov, A. L. Rheingold, F. N. Castellano and L. X. Chen, *J. Phys. Chem. A*, 2010, **114**, 12780-12787.
82. S. Cho, M. W. Mara, X. Wang, J. V. Lockard, A. A. Rachford, F. N. Castellano and L. X. Chen, *J. Phys. Chem. A*, 2011, **115**, 3990-3996.
83. S. E. Brown-Xu, M. S. J. Kelley, K. A. Fransted, A. Chakraborty, G. C. Schatz, F. N. Castellano and L. X. Chen, *J. Phys. Chem. A*, 2016, **120**, 543-550.
84. K. Haldrup, A. O. Dohn, M. L. Shelby, M. W. Mara, A. B. Stickrath, M. R. Harpham, J. Huang, X. Zhang, K. B. Møller, A. Chakraborty, F. N. Castellano, D. M. Tiede and L. X. Chen, *J. Phys. Chem. A*, 2016, **120**, 7475-7483.
85. A. Chakraborty, J. C. Deaton, A. Haeefe and F. N. Castellano, *Organometallics*, 2013, **32**, 3819-3829.
86. M. Han, Y. Tian, Z. Yuan, L. Zhu and B. Ma, *Angew. Chem. Int. Ed.*, 2014, **53**, 10908-10912.
87. C. Zhou, Y. Tian, Z. Yuan, M. Han, J. Wang, L. Zhu, M. S. Tameh, C. Huang and B. Ma, *Angew. Chem. Int. Ed.*, 2015, **54**, 9591-9595.
88. C. Zhou, L. Yuan, Z. Yuan, N. K. Doyle, T. Dilbeck, D. Bahadur, S. Ramakrishnan, A. Dearden, C. Huang and B. Ma, *Inorg. Chem.*, 2016, **55**, 8564-8569.
89. Y.-Z. Ma, C. Zhou, B. Doughty, D. C. Easley, J. Deterding and B. Ma, *Chem. Eur. J.*, 2017, **23**, 17734-17739.
90. B.-C. Tzeng, W.-F. Fu, C.-M. Che, H.-Y. Chao, K.-K. Cheung and S.-M. Peng, *J. Chem. Soc., Dalton Trans.*, 1999, **0**, 1017-1024.
91. M. Kato, A. Omura, A. Toshikawa, S. Kishi and Y. Sugimoto, *Angew. Chem. Int. Ed.*, 2002, **41**, 3183-3185.
92. V. Sicilia, P. Borja, J. M. Casas, S. Fuertes and A. Martín, *J. Organomet. Chem.*, 2013, **731**, 10-17.
93. V. Sicilia, J. Forniés, J. M. Casas, A. Martín, J. A. López, C. Larraz, P. Borja, C. Ovejero, D. Tordera and H. Bolink, *Inorg. Chem.*, 2012, **51**, 3427-3435.
94. Z. Wang, L. Jiang, Z.-P. Liu, C. R. R. Gan, Z. Liu, X.-H. Zhang, J. Zhao and T. S. A. Hor, *Dalton T.*, 2012, **41**, 12568-12576.
95. E. A. Katlenok and K. P. Balashev, *Opt. Spectrosc.*, 2014, **117**, 374-380.
96. E. A. Katlenok, A. A. Zolotarev and K. P. Balashev, *Russ. J. Gen. Chem.*, 2014, **84**, 1593-1598.
97. W. Xiong, F. Meng, C. You, P. Wang, J. Yu, X. Wu, Y. Pei, W. Zhu, Y. Wang and S. Su, *J. Mater. Chem. C*, 2019, **7**, 630-638.
98. S. Develay and J. A. G. Williams, *Dalton T.*, 2008, **0**, 4562-4564.
99. Z. Guo and M. C. W. Chan, *Chem. Eur. J.*, 2009, **15**, 12585-12588.
100. Z. Guo, S. M. Yiu and M. C. Chan, *Chemistry*, 2013, **19**, 8937-8947.
101. A. Chakraborty, J. E. Yarnell, R. D. Sommer, S. Roy and F. N. Castellano, *Inorg. Chem.*, 2018, **57**, 1298-1310.
102. Y. Zhu, K. Luo, X. Li, H. Wang, C. Yang, H. Ni and Q. Li, *J. Lumin.*, 2018, **204**, 296-302.
103. R. M. van der Veen, A. Cannizzo, F. van Mourik, A. Vlcek and M. Chergui, *J. Am. Chem. Soc.*, 2011, **133**, 305-315.
104. P. Kim, M. S. Kelley, A. Chakraborty, N. L. Wong, R. P. Van Duyne, G. C. Schatz, F. N. Castellano and L. X. Chen, *J. Phys. Chem. C*, 2018, **122**, 14195-14204.
105. M. Yoshida and M. Kato, *Coord. Chem. Rev.*, 2018, **355**, 101-115.
106. H. Xiang, J. Cheng, X. Ma, X. Zhou and J. J. Chruma, *Chem. Soc. Rev.*, 2013, **42**, 6128-6185.
107. K. Masako, *Bull. Chem. Soc. Jpn.*, 2007, **80**, 287-294.
108. A. Kobayashi and M. Kato, *Eur. J. Inorg. Chem.*, 2014, **2014**, 4469-4483.
109. J. A. Gareth Williams, S. Develay, D. L. Rochester and L. Murphy, *Coord. Chem. Rev.*, 2008, **252**, 2596-2611.
110. S. Kaori, H. Yuji, T. Hisakazu, K. Tamami and K. Masako, *JPN J. Appl. Phys.*, 2005, **44**, L500.
111. J. Yu, X. Wu, H. Tan, Y. Liu, Y. Wang, M. Zhu and W. Zhu, *Sci. China Chem.*, 2013, **56**, 1137-1142.
112. X. G. Wu, Y. Liu, Y. F. Wang, L. Wang, H. Tan, M. X. Zhu, W. G. Zhu and Y. Cao, *Org. Electron.*, 2012, **13**, 932-937.
113. Y. Zhu, K. Luo, L. Zhao, H. Ni and Q. Li, *Dyes Pigm.*, 2017, **145**, 144-151.
114. W. Xiong, F. Meng, H. Tan, Y. Wang, P. Wang, Y. Zhang, Q. Tao, S. Su and W. Zhu, *J. Mater. Chem. C*, 2016, **4**, 6007-6015.
115. B. Ma, P. I. Djurovich, S. Garon, B. Alleyne and M. E. Thompson, *Adv. Funct. Mater.*, 2006, **16**, 2438-2446.
116. N. Su, F. Y. Meng, J. H. Chen, Y. F. Wang, H. Tan, S. J. Su and W. G. Zhu, *Dyes Pigm.*, 2016, **128**, 68-74.
117. J. Yu, J. Luo, Q. Chen, K. He, F. Meng, X. Deng, Y. Wang, H. Tan, H. Jiang and W. Zhu, *Tetrahedron*, 2014, **70**, 1246-1251.
118. X. H. Yang, J. D. Froehlich, H. S. Chae, B. T. Harding, S. Li, A. Mochizuki and G. E. Jabbour, *Chem. Mater.*, 2010, **22**, 4776-4782.
119. X. Yang, B. Jiao, J.-S. Dang, Y. Sun, Y. Wu, G. Zhou and W.-Y. Wong, *ACS Appl. Mater. Interfaces*, 2018, **10**, 57695.

## ARTICLE

## Journal Name

120. A. Tronnier and T. Strassner, *Dalton T.*, 2013, **42**, 9847-9851.
121. S. Yang, F. Meng, X. Wu, Z. Yin, X. Liu, C. You, Y. Wang, S. Su and W. Zhu, *J. Mater. Chem. C*, 2018, **6**, 5769-5777.
122. M. Z. Shafikov, R. Daniels, P. Pander, F. B. Dias, J. A. G. Williams and V. N. Kozhevnikov, *ACS Appl. Mater. Interfaces*, 2019, **11**, 8182-8193.
123. Y.-Z. Chen, D. Pan, B. Chen, G.-X. Wang, C.-H. Tung and L.-Z. Wu, *Eur. J. Inorg. Chem.*, 2017, **2017**, 5108-5113.
124. T. R. Cook, Y. Surendranath and D. G. Nocera, *J. Am. Chem. Soc.*, 2009, **131**, 28-29.
125. D. Preston, J. J. Sutton, K. C. Gordon and J. D. Crowley, *Angew. Chem. Int. Ed.*, 2018, **57**, 8659-8663.
126. M. Albrecht and G. van Koten, *Angew. Chem. Int. Ed.*, 2001, **40**, 3750-3781.

TOC



Platinum (II) binuclear complexes with two metal centers facing each other are reviewed on their molecular structures, photophysical properties, and applications in light emitting and sensing devices.